



**Faculty of Engineering**  
Cairo University



---

## **Smart Shunt For treatment Of Hydrocephalus**

---

submitted to:  
**NILE UNIVERSITY**

submitted by:  
**Mohamed Ahmed Abdelaziz**  
**Mohamed Abdelkarim Ibrahim Seyam**  
**Ramadan Ibrahim Moheyeldeen**

# Contents

<b>1 Abstract</b>	<b>3</b>
<b>2 Introduction</b>	<b>3</b>
<b>3 over view on shunt hardware,hydrocephalus &amp; equations model</b>	<b>4</b>
3.1 Mathematical Model Dynamic Of CSF Dynamics . . . . .	4
3.2 Model Of CSF & blood Pathway . . . . .	5
3.3 Cyclic Motion Of Choroid Plexus Follow Cardiac Cycle By Forcing Function	6
3.4 Acceleration Of Elastic Tissue . . . . .	6
3.5 Continuity Of CSF Flow In The Ventricles . . . . .	7
3.6 Axial Momentum Along The Streamline In The flow direction . . . . .	7
3.7 Continuity of CSF Flow In SAS Without Choroid Plexus Effect . . . . .	8
3.8 Diffusive Reabsorption Of CSF $q_{e,j}$ In SAS . . . . .	8
<b>4 methodology</b>	<b>10</b>
4.1 Scenario . . . . .	10
<b>5 Component</b>	<b>11</b>
5.1 Telemetry Transducer . . . . .	12
5.2 The Sensors Leads . . . . .	12
5.3 schematic . . . . .	12
<b>6 telemetry flow sensor</b>	<b>13</b>
6.1 The principle Of Working . . . . .	13
6.1.1 Basics Of Fluid Dynamics . . . . .	13
6.1.2 MEME Flow Rate Sensor . . . . .	14
6.1.3 Design And Readings . . . . .	14
6.2 materials & methods . . . . .	15
6.2.1 transducer description . . . . .	15
6.2.2 Power Management In The Implant . . . . .	17
6.2.3 external reading unit . . . . .	18
6.2.4 Packing Of The Transducer And Biocompatibility . . . . .	18
6.3 Test Liquids For Characterization Of Protein Adsorption . . . . .	19
6.4 Results . . . . .	19
6.5 Accuracy, Precision, And Uncertainty . . . . .	22
<b>7 Intercranial Pressure meme sensor</b>	<b>22</b>
7.1 Device Design . . . . .	23
7.1.1 Components . . . . .	23

7.1.2	Fabrication . . . . .	24
7.1.3	calibration . . . . .	24
7.2	principle of working of pressure sensor . . . . .	25
<b>8</b>	<b>micro capacitive tilt sensor</b>	<b>26</b>
8.1	Initial Design . . . . .	26
8.2	Principle of working . . . . .	27
8.3	Digital Sensor . . . . .	29
8.4	Resolution, Precision, And Accuracy . . . . .	31
<b>9</b>	<b>Wireless body communication</b>	<b>32</b>
9.1	Art of in vivo communication . . . . .	32
9.2	In vivo channel modeling and characterization . . . . .	33
9.3	Wireless powering of medical sensors . . . . .	35
9.3.1	The effect of the environment . . . . .	36
9.3.2	Experimental results . . . . .	36
<b>10</b>	<b>discussion</b>	<b>37</b>
<b>11</b>	<b>conclusion</b>	<b>37</b>

## 1 Abstract

smart shunt will provide better care and ease for both the patient and the doctor as it will provide the necessary data for diagnosing the shunt failure and separate it from other illnesses like flu. it also will provide accurate readings for future development of the shunt and solving its failure causes. the shunt may cause over drainage and we could assess to stabilize the patient by providing guidance to his position without rushing to the hospital every single time . it also could alert the patient to change his position before serious passive effects .all of this would be done with the data coming from pressure sensor ,flow sensor and tilt sensor with an efficient way of powering the implant and transmitting the data.

The reading from the tilt sensor ensure the patient position to alert him to change his posture if the ICP or flow rate(overdrainage) increase that may be caused by shunt failure and cause coma, stroke, seizure, or even death. The device harvest its power thought RF antenna and additional electronics to power the device and transmit the data.

Flow sensing transducer for monitoring CSF flow is based on measuring heat dissipation of local thermal source. The sensor use passive telemetry for power supply and data transmission.

It is very important to determine human positions so that we will explain two tilt sensors based on MEMS (Micro-electromechanical Systems) and variable capacitors, and we can take advantage of the ground gravity to determine the position of the human body, the first device can determine with range (-90° to 90°), Based on the same concept, the second one is the digital sensor.

## 2 Introduction

Hydrocephalus is a common congenital disorder of CNS that may be presented in one out of 500 to 2000 child. It is also presented due to aging which cause dementia and gait problems. CSF production rate is 20 ml/h if it is not absorbed properly it causes hydrocephalus.The main treatment is a **SHUNT** placement(100,000 surgery per year). Shunt blockage in the first year ranges from 20% to 30%. For diagnoses on an invasive procedure is used if not sure surgery for replacement is preferred, but this could be very expensive.

ICP capacitive sensing can provide pressure measurement, but the flow sensing provide an efficient way for diagnostic for The blockage of the shunt, over-drainage, and under-drainage with much cheaper,safer, and 24/7 remote monitoring system compared to the current technologies(e.g. MRI, CFD or ultrasound with contrast). This continuous readings could lead to a better understanding of hydrocephalus treatment and better quality of life for the patients.

The reading from the tilt sensor ensure the patient position to alert him to change his posture if the ICP or flow rate(overdrainage) increase that may be caused by shunt failure and cause coma, stroke, seizure, or even death. The device harvest its power thought RF antenna and additional electronics to power the device and transmit the data.

### 3 over view on shunt hardware,hydrocephalus & equations model

#### 3.1 Mathematical Model Dynamic Of CSF Dynamics

$$CSF_{production} + CSF_{externalinfusion} = CSF_{storage} + CSF_{reabsorption}$$

- $CSF_{production}$  is almost constant
- $CSF_{external infusion}$  is the artificial CFS added.
- $CSF_{reabsorption} = \frac{p - p_{ss}}{R}$  where  $p$  is the CSF pressure,  $P_{ss}$  is the pressure on the sagittal sinus.
- $CSF_{storage} = c \frac{dp}{dt}$  where  $c$  is the cerebrospinal compliance. ( $mm/Hgml^{-1}$ )  
the cerebrospinal compliance is rely on two factor.the cerebral elestance ( $E$ ) and the reference pressure ( $P_0$ )  $\rightarrow c = \frac{1}{E(p - p_0)}$ .  
this equation reflects that the compliance of the brain decreases when CSF pressure increases.

combining equation together we get

$$\frac{1}{E(p - p_0)} \cdot \frac{dp}{dt} \cdot \frac{p - p_b}{R} = I(t)$$

- $I(t) \Rightarrow$  rate of external volumeaddition
- $P_b \Rightarrow$  baseline pressure

it can be solved for various types of external volume addition . the most common

1. constant infusion of CSF ( $i(t) = 0$  for  $t < 0$  and  $i(t) = I_{inf}$  for  $t > 0$ ) we can match the real curve by this equation

$$p(t) = \frac{\left[ I_{inf} + \frac{P_b - P_0}{R} \right] \cdot [P_b - P_0]}{\frac{P_b - P_0}{R} + I_{inf} \cdot e^{(-E[\frac{P_b - P_0}{R} + I_{inf}]) \cdot t}} + p_0$$

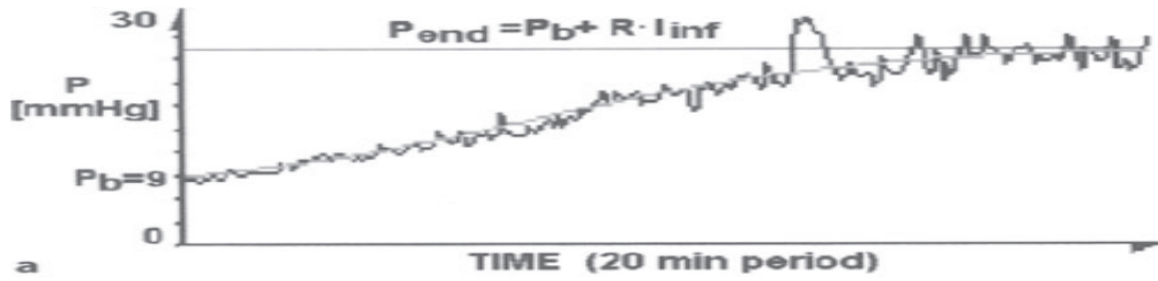


Figure 1: pressure recording during infusion test

## 2. abolus infection of CSF ( volume $\delta V$ )

- purposes

- calculating  $PVI$  pressure volume index . it is defined as the volume added externally to produce a ten fold increase in pressure.  $PVI = \frac{1}{43 \cdot E}$  and if it is less than  $13ml$  indicates that pressure volume compensatory reverse isn't sufficient. and if it is greater than  $26ml$  it indicates over compliant brain.
- important in theoretical calculation of the relation between the pulse wave amplitude of ICP and mean CSF pressure.
- describe the relation between the net effective volume increase and  $P_{csf}$  (pressure volume curve) by substituting with  $t=0$  in the general equation that give

$$P = (P - P_0) \cdot e^{E\delta V} + P_0$$

## 3.2 Model Of CSF & blood Pathway

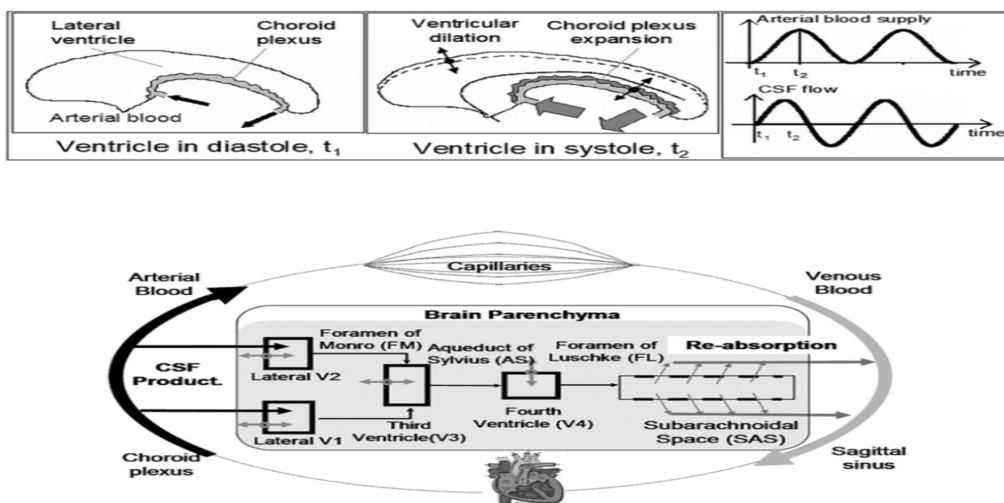


Figure 2: schematic of CSF pathway and vascular system

### 3.3 Cyclic Motion Of Choroid Plexus Follow Cardiac Cycle By Forcing Function

$$\mathbf{a}(t) = \alpha \left( 1.3 + \sin(\omega t - \frac{\pi}{2}) - \frac{1}{2} \cos(2\omega t - \frac{\pi}{2}) \right)$$

where:

- $\mathbf{a}(t)$  choroid plexus displacement[m].
- $\alpha$  amplitude of choroid expansion [m].
- $\omega$  heart rate frequency [rad/s].

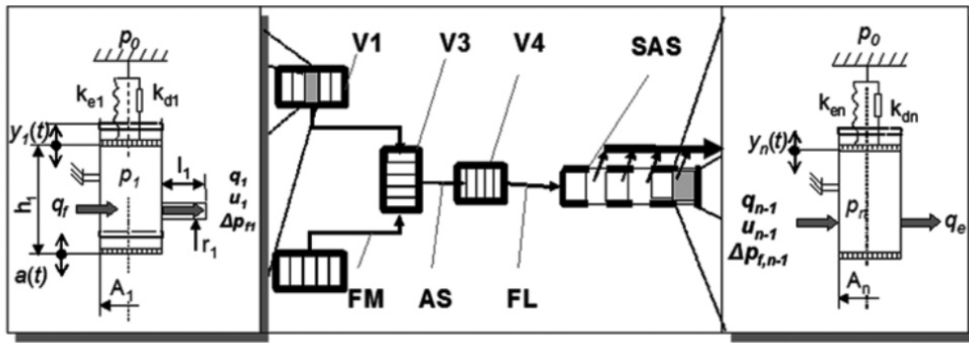


Figure 3: model of CSF flow induced by choroid plexus

### 3.4 Acceleration Of Elastic Tissue

$$\rho_\omega A_i \delta \frac{\partial^2 y_i(t)}{\partial t^2} + K_d \frac{\partial y_i(t)}{\partial t} + K_e y_i(t) - A_i [P_i(t) - P_o(t)] = 0, i \in LV_1 - LV_4, SAS$$

, where:

- $\rho_\omega$  tissue density [ $K_g/m^3$ ].
- $A_i$  cross section of the ventricles or subarachnoid
- $\delta$  tissue width[m].
- $y_i(t)$  tissue displacement in the section [m].
- $k_d$  tissue compliance [ $N S /m$ ].
- $k_e$  tissue elasticity constant[N/m].
- $P_o(t)$  pressure of brain parenchyma [ $N/m^2$ ].
- $P_i(t)$  CSF pressure in ventricles and subarachnoid section(ICP) [ $N/m^2$ ].

- $L_i$  length of foramen connecting ventricles[m].
- $V_i(t)$  axial CSF flow velocity[m/s].
- **SAS** sub arachnoid section.

### 3.5 Continuity Of CSf Flow In The Ventricles

$$\frac{\partial[A_i[h_i + a(t)] + y_i(t)]}{\partial t} = q_{f,i} - q_i, i \in LV_1 - LV_4$$

where:

- $A_i$  cross section of the ventricles or subarachnoid
- $h_i$  height of the ventricles or subarachnoid section[m].
- $a(t)$  choroid plexus displacement[m].
- $y_i(t)$  tissue displacement in the section [m].
- $q_{f,i}(t)$  CSf production rate in choroid plexus [ $m^3/s$ ].
- $q_i(t) = A_i V_i$  CSf flow rate leaving ventricles [ $m^3/s$ ].
- $L_i$  length of foramen connecting ventricles[m].
- $V_i(t)$  axial CSF flow velocity[m/s].

### 3.6 Axial Momentum Along The Streamline In The flow direction

It is valid for axial CSF flow velocity.

$$\rho \left[ \frac{\partial v_i}{\partial t} + v_i \frac{\partial v_i}{\partial z} \right] + \frac{\partial P_i(t)}{\partial z} = -F_i, i \in FM, AS, Fl$$

$$F_i = \frac{8\mu}{r_i^2} v_i$$

,where

- $V_i(t)$  axial CSF flow velocity[m/s].
- $P_i(t)$  CSF pressure in ventricles and subarachnoid section(ICP) [ $N/m^2$ ].
- $F_i$  poiseuille friction [ $N/m^3$ ].
- $\mu$  fluid viscosity[Pa s].
- $r_i$  radius of foramine [m].

### 3.7 Continuity of CSF Flow In SAS Without Choroid Plexus Effect

$$\frac{\partial(A_j[h_j + y_i(t)])}{\partial t} = q_{j,i} - q_{e,j}, j \in SAS$$

,where:

- $A_i$  cross section of the ventricles or subarachnoid section [ $m^2$  ].
- $h_i$  height of the ventricles or subarachnoid section [m].
- $q_{f,i}(t)$  CSF production rate in choroid plexus [ $m^3/s$  ].
- $q_i(t) = A_i V_i$  CSF flow rate leaving ventricles [ $m^3/s$  ].
- $y_i(t)$  tissue displacement in the section [m].

### 3.8 Diffusive Reabsorption Of CSF $q_{e,j}$ In SAS

$$q_{e,j} = \kappa[P_j(t) - P_o(t)], j \in SAS$$

,where:

- $\kappa$  reabsorption constant [ $m^3/Pas$  ].
- $P_o(t)$  pressure of brain parenchyma [ $N/m^2$  ].
- $P_i(t), P_{SAS}(t)$  CSF pressure in ventricles and subarachnoid section (ICP) [ $N/m^2$  ].

TABLE I  
TISSUE AND FLUID PROPERTIES

Property	Value	Source
Young Modulus for ventricles	2,100 N/m <sup>2</sup>	[27]
Young Modulus for SAS	3,500 N/m <sup>2</sup>	Derived from [28]
Fluid density, $\rho_f$	1,004 - 1,007 kg/m <sup>3</sup>	[29]
Fluid viscosity, $\mu$	$10^{-3}$ Pa s	i.e. water
Spring elasticity, $k_e$	8 N/m (normal)	Extracted
Brain Dampening, $k_d$	$0.35 \times 10^{-3}$ (N s)/m	Assumed - low dampening effect
Ependyma density, $\rho_w$	1,000 kg/m <sup>3</sup>	i.e. water
Reabsorption constant, $\kappa$	$1.067 \times 10^{-11}$ m <sup>3</sup> /(Pa s)	Estimated

Figure 4: tissue and fluid properties

The shunt is formed of a reservoir, a proximal & distal catheter, gravitational device or a siphoning chamber. opening pressure on lying and standing is provided in fig5.

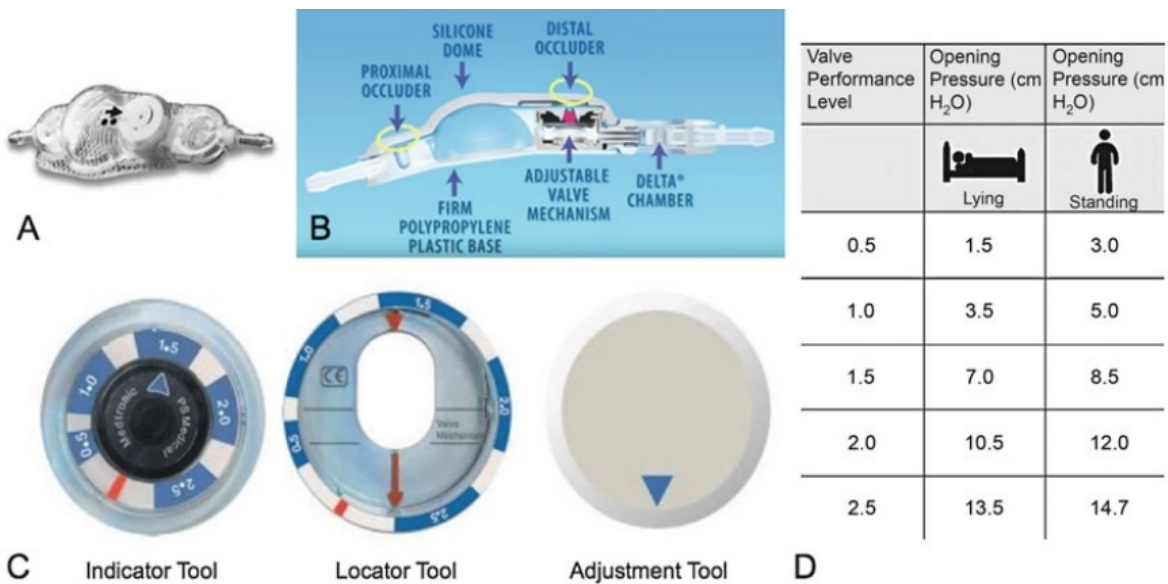


Figure 5: the typical shunt design with opening pressure values on lying and standing

An adjustment kit for the modifications done on the shunt to maintain easy adjustment without invasive procedure. fig6 show different performance levels.

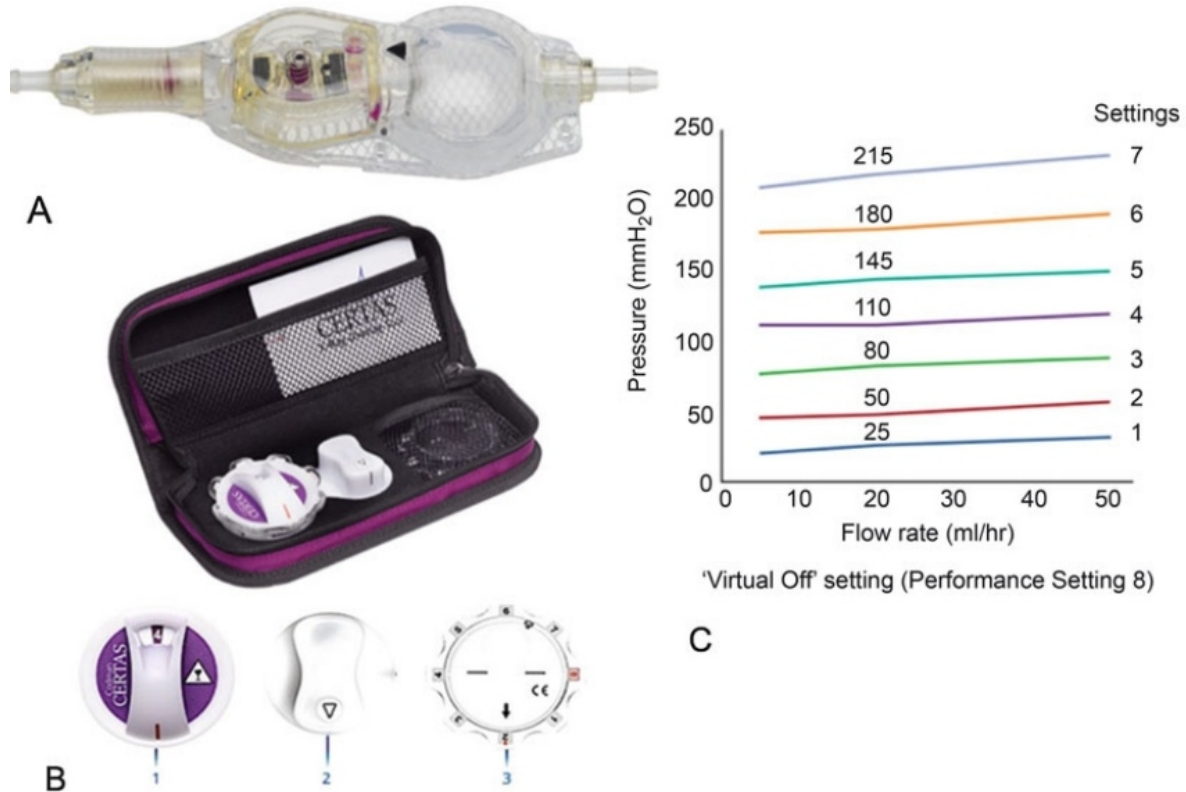


Figure 6: adjustment kit with different operating opening pressure settings

Fig7 show design of the shunt with programmable servo motor for adjustment using a

coded magnet signal from the adjustment kit.

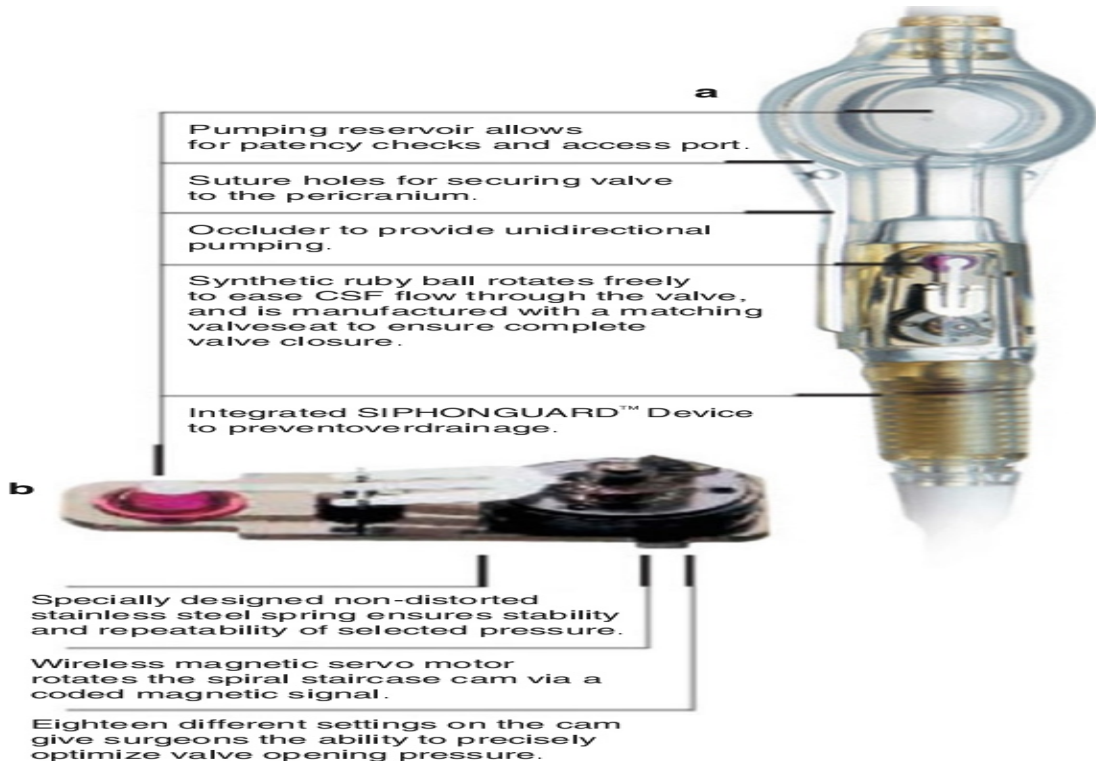


Figure 7:

## 4 methodology

The sensors will be implanted near the shunt sealed to distal catheter. The device will harvest power to work from external unit with the help of RF technology. telemetry electronics, load modulator, RF-DC converter are used in the implant to supply the circuit with the required voltage. Feedback between the implant and the external unit will regulate the data transmission and RF transmission rates to keep the temperature at an optimal rates, Pressure, flow, and tilt data are transmitted to the external unit with Bluetooth to be processed. If any of the readings exceed the normal limits, the patient will be alerted and given some instruction like sitting or lying down for a period of time. The doctor will be alerted to view the data and make adjustment to the valve or tell the patient to go to the hospital. These adjustments may be performed automatically.

### 4.1 Scenario

The flow rate increase over 25 ml/h for a period longer than an hour(overdrainage) with the patient standing position confirmed by the tilt sensor. The patient will be asked to sit or lay down for a period of time to reduce the overdrainage effect, if no change the doctor

will be informed to do adjustments on the valve remotely by the kit with the patient at home who place it on the shunt with some guidance provided on a mobile application for displaying the data and communicating with the doctor. The wireless magnet servo motor rotates to a new opening pressure setting by a coded magnetic signal see fig???. fig?? contain the kit used usually in hospitals, but in our case the doctor perform the adjustments remotely. Opening pressure for lying and standing are provided in fig??. other scenarios may be present like blockage, underdrainage, and ICP increase similar approaches with some modifications will be used. The general idea is presented in the scenario above.

## 5 Component

the implanted measurement system consist of

- A telemetry monitor implanted under the skin
- A multiple leads with sensors implemented in the brain.
- Radio Frequency telemetry link
- personal computer program.
- external reference for the measured component

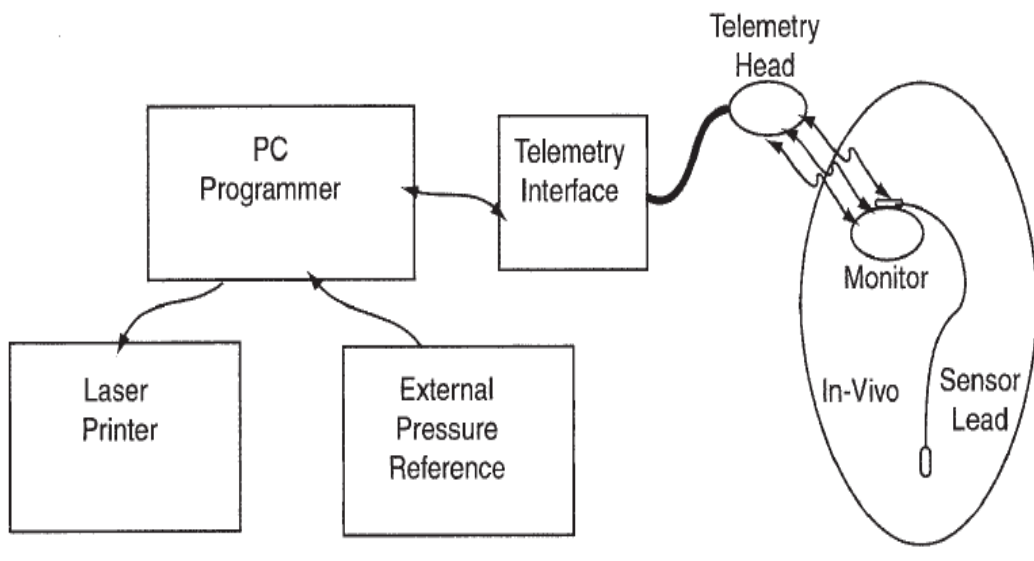


Figure 8: implantable monitoring system

## 5.1 Telemetry Transducer

the telemetry monitor consist of

- Lithium–manganese dioxide power source.
- Radio frequency transmission coil hermetically sealed within a titanium can to transmit the signals to the telemetry head and then to the programmable.
- 128 kb of memory to store the data coming from the signal and using data compression algorithm to compress the data.

## 5.2 The Sensors Leads

there are two implanted sensors to provide data from the brain.

- pressure sensor to monitor intercranial pressure interms of mm/Hg
- flow sensor to monitor the flow condition of cerebro spinal fluid in and out of the valve shunt.

and there is a tilt sensor to provide the data about patient case if he stand ,sit ,sleep ,moving fast ....etc.

## 5.3 schematic

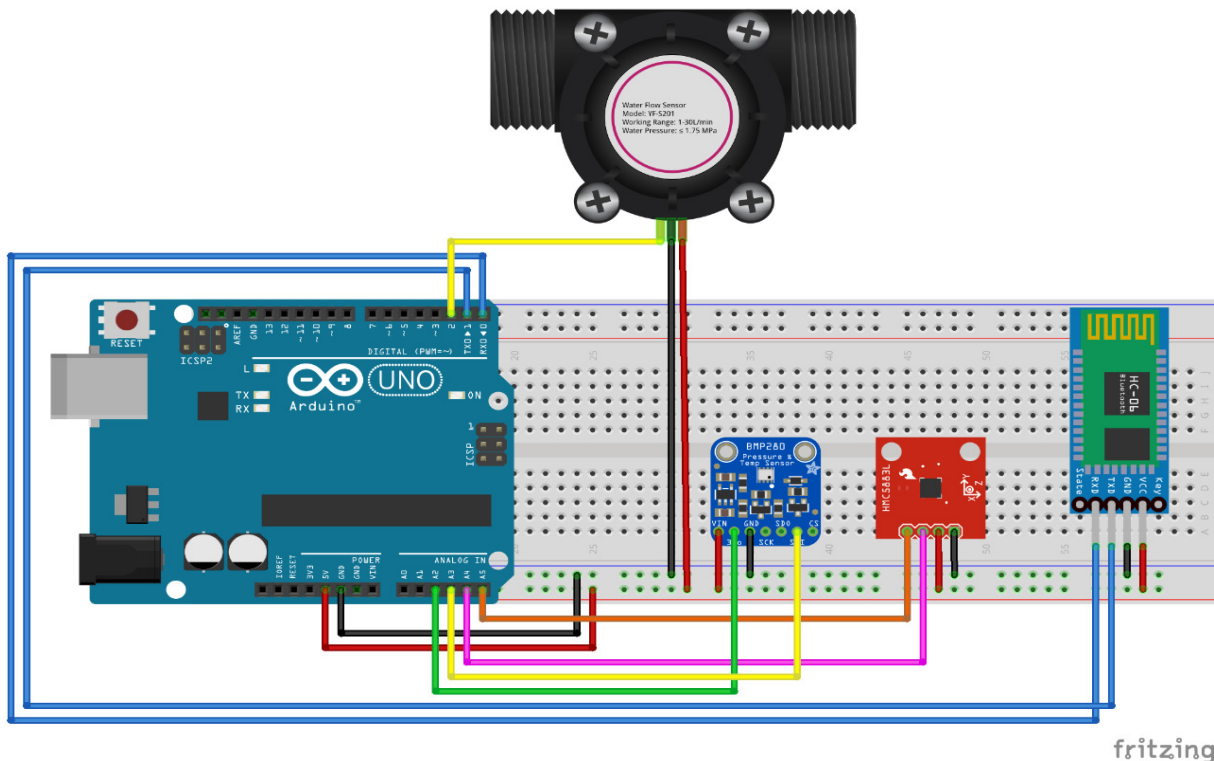


Figure 9: schematic for the smart shunt

## 6 telemetry flow sensor

### 6.1 The principle Of Working

It is based on the amount of heat removed from a heat temperature sensor. It is modeled using heat transfer in liquids.

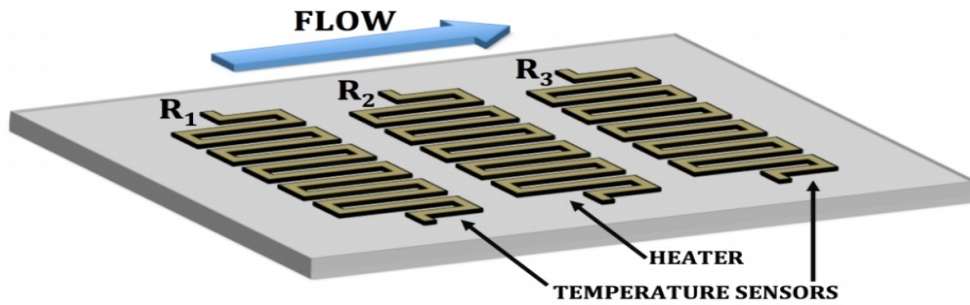


Figure 10: calorimetric flow sensor

R2 act as a heater and R1 & R3 act as temperature sensors to determine the velocity of the flow and its direction.

#### 6.1.1 Basics Of Fluid Dynamics

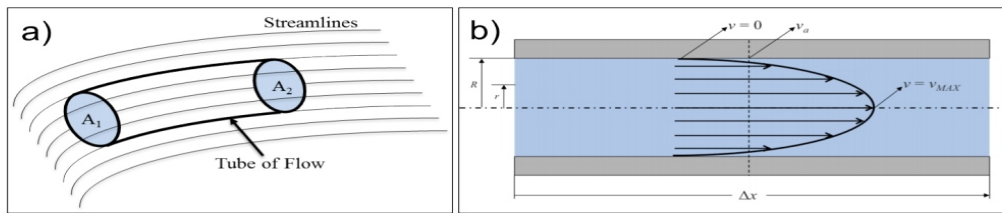


Figure 11: (a)tube (b)velocity profile

$$\text{The volume of fluid} = \frac{V}{\Delta t} = \int \frac{\Delta x}{\Delta t} dA = \int v dA$$

- $\Delta x$  displacement
- $\Delta t$  time interval
- A cross section area
- V volume

$$\text{Average velocity } v_a = \frac{\int v dA}{A}, \text{Flow rate } Av_a = \int v dA$$

Temperature and pressure may affect the readings.

### 6.1.2 MEME Flow Rate Sensor

The advantages of this type is that it has better precision, low power consumption, rapid response, and low cost. It is most useful in microfluidic devices with low velocities.

### 6.1.3 Design And Readings

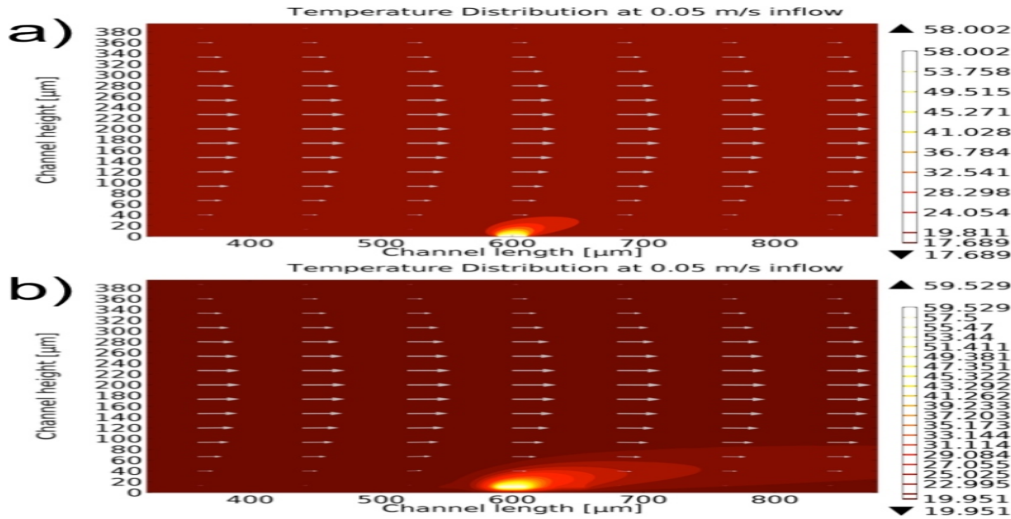


Figure 12: design of calorimeter with height  $400\mu\text{M}$

A PMMA (polymethylmethacrylate) platform has better temperature distribution profile because it allow for a higher flow velocity of the fluid, especially in very slow fluids.

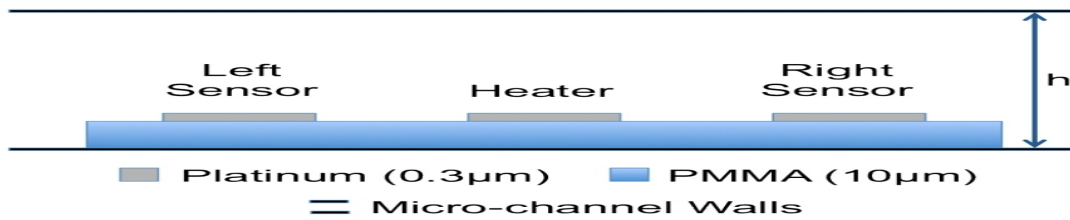


Figure 13: (a)no PMMA CFD model (b)PMMA CFD model

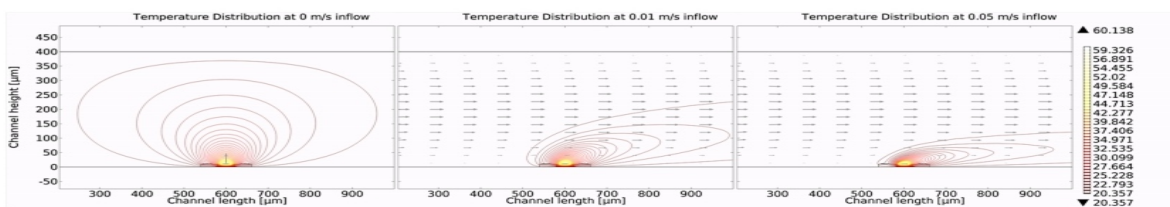


Figure 14: temperature distribution with different flow rates

The readings from the two sensors present the flow rate due to temperature change on both sensors.

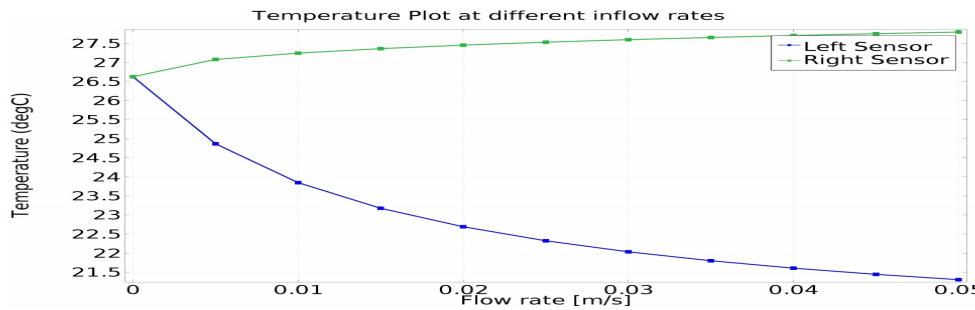


Figure 15: temperature at different flow rates

## 6.2 materials & methods

The implanted transducer will be glued and sealed into atrial catheter. External device supply the power to the sensor by passive telemetry and then transmit this data with Bluetooth to a computer or data storage device.

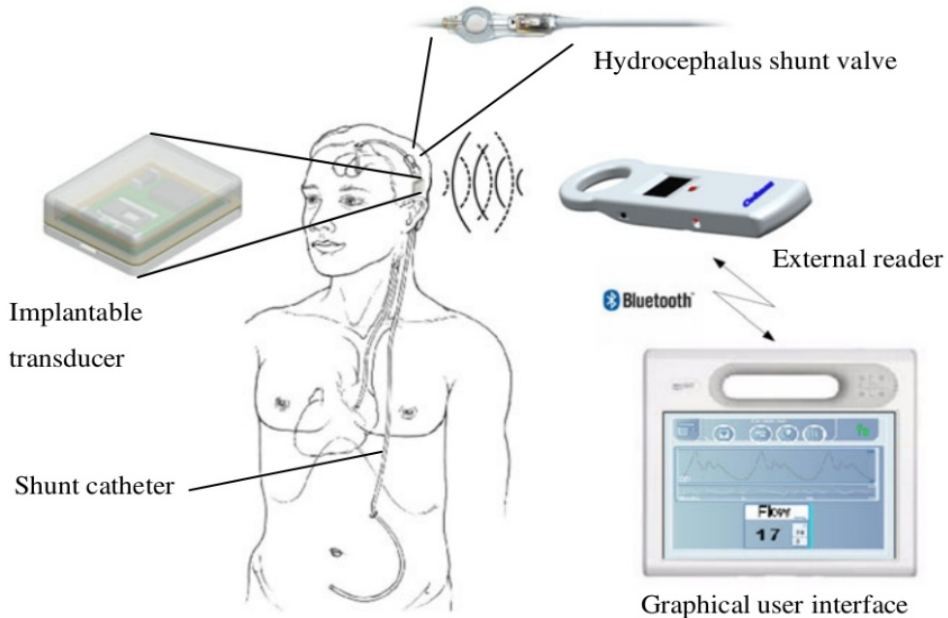


Figure 16: implantable transducer and external energy unit

### 6.2.1 transducer description

The transducer consist of three main parts

- Calorimetric flow sensor (based on thermal anemometer principle).
- Microprocessor.

- RF section.

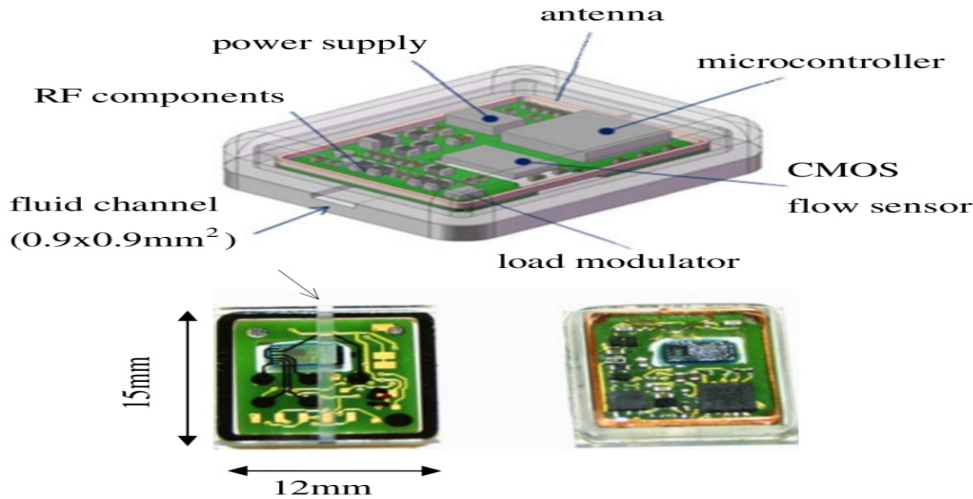


Figure 17: components of the transducer

The CMOS chip contain the sensor and all necessary electronics

- ADC.
- Linearization amplifier.
- Temperature compensation.
- Calibration memory.
- Power supply.
- Antenna.
- Load Modulator.
- Flow channel.

The calibration is done by using water medium (artificial CSF) for a flow between 2 ml/h and 40 ml/h with addition of 10% fresh blood or increase protein content in the fluid.

The RF section (13.56 MHZ) extract energy for the implant, RF induced voltage to the microcontroller and modulation of FSK signal to communicate with the external unit. 109 KHZ for logic 0 & 117 KHZ for logic 1 are applied to the load modulation circuit by the microcontroller.

### 6.2.2 Power Management In The Implant

To reduce the energy dissipation some considerations should be used:

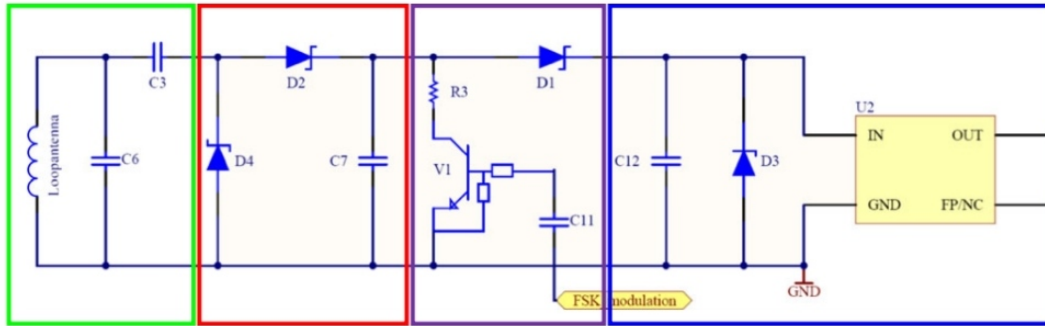


Figure 18: transducer telemetry electronics

- Green box: loop antenna and impedance matching.
- Red box: RF-DC converter.
- Purple box: load modulator.
- Blue box Dc supply.
- RF-DC converter output is passed to voltage regulator which is used to supply 3.3 V to the CMOS flow sensor.
- Minimum energy for the implant is 19.17 mW
  - 16.3 mW by the CMOS sensor.
  - 2.87 mW by the microcontroller.
- Large capacitor used in DC supply unit (C12) to stable the power supply during load modulation.
- In load modulator:
  - R3 is small and limited by collector current to ensure maximum load modulation amplitude.
  - C11 is used to adjust the modulation pulse.
- If pulse width is large, energy dissipation in R3 is increased and the range of telemetry is reduced.
- If the pulse width is small, the FSk signal will not be detected by the external unit.
- 15% to 20% duty cycle has the best results.
- Diodes is used instead of inductivity used in most telemetry to reduce the thickness of the implant.

### 6.2.3 external reading unit

### 6.2.4 Packing Of The Transducer And Biocompatibility

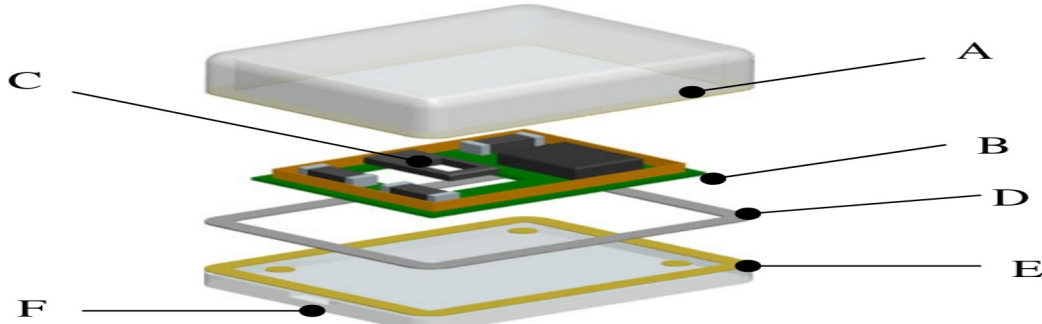


Figure 19: (A)glass cap (B)electronics (C)flow sensor (D)braze ring (E)glass base (F)flow channel

The calorimetric flow sensor is enclosed by borosilicate glass 100 $\mu m$  thickness. The heater and temperature sensor is not exposed to the body fluids providing long term biocompatible implant that last for more than 10 years.

Some design considerations should be taken to lower the energy dissipation:

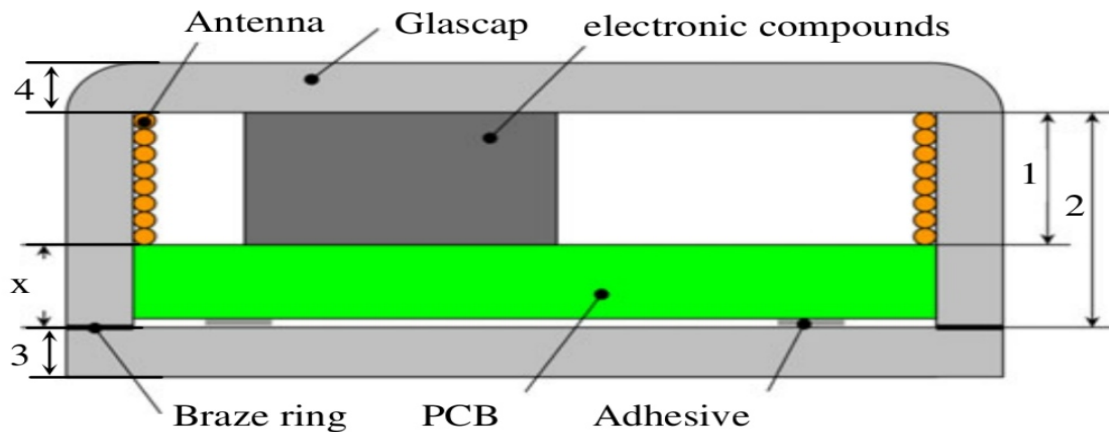


Figure 20: (1)antenna height 1 mm (2)height for electronics 2 mm (3)(4)bottom base and cap 1.5 mm (x)distance between antenna and brazing ring .7 mm

The .7 mm between antenna and brazing ring cause damping of 20 dB which lead to maximum communication distance 37 mm.

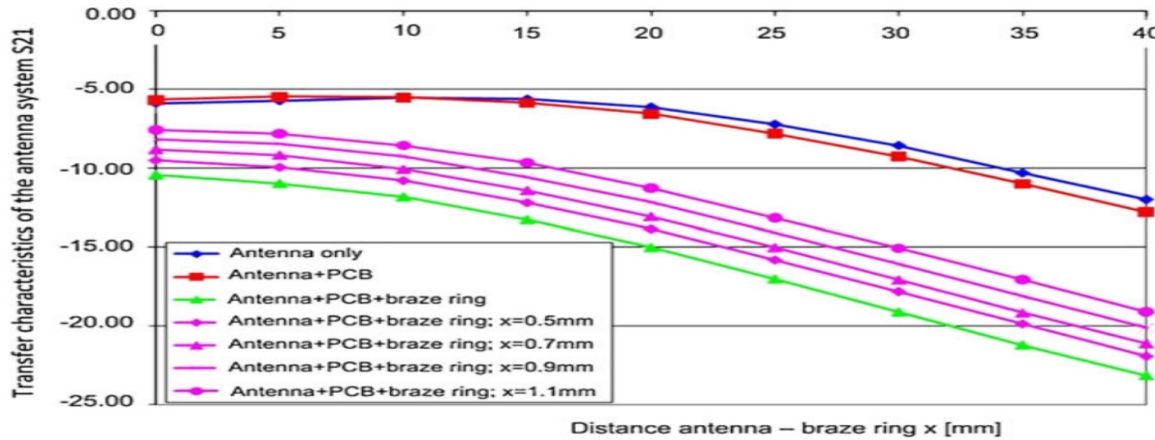


Figure 21: transfer characteristics between implant and external unit

### 6.3 Test Liquids For Characterization Of Protein Adsorption

Elevated protein concentration in the CSF and blood component adsorption cause shunt blockage and inflammation. The major protein film observed is albumin then fibrinogen and fibronectin after insertion of the shunt. Simulations were made using artificial CSF and fresh human blood to see the effect of protein deposition on the sensor.

Chemical Name	Formula	Conc. in CSF [g/L]
Sodium chloride	NaCl	8.660
Potassium chloride	KCl	0.224
Calcium chloride dihydrate	CaCl <sub>2</sub> -2H <sub>2</sub> O	0.206
Magnesium chloride hexahydrate	MgCl <sub>2</sub> -6H <sub>2</sub> O	0.163
Sodium phosphate monobasic monohydrate	NaH <sub>2</sub> PO <sub>4</sub> -H <sub>2</sub> O	0.027
Di-Sodium hydrogen phosphate heptahydrate, a/cs	Na <sub>2</sub> HPO <sub>4</sub> -7H <sub>2</sub> O	0.214
Sodium Azide 0.1 M Solution	N <sub>3</sub> Na	5 g or 0.77 ml
D-(+)-Glucose	C <sub>6</sub> H <sub>12</sub> O <sub>6</sub>	0.600
Urea	CH <sub>4</sub> N <sub>2</sub> O	0.201
Albumin (from human serum)		2.000
Gamma-globulin from human blood		0.015

Figure 22: compositions of artificial CSF

### 6.4 Results

Three sensors are used to measure the relative flow rate with reference to flow rate measurement taken by a scale.

$$\text{relative flow rate} = \frac{\text{flow rate(sensor)} - \text{flow rate(scale)}}{\text{flow rate(scale)}} \times 100\%$$

different scenarios are presented to improve accuracy, precision, and reliability of the sensor with calibrating the sensor once at 22°C and also at 37°C, also different fluids were

used with different flow rates.

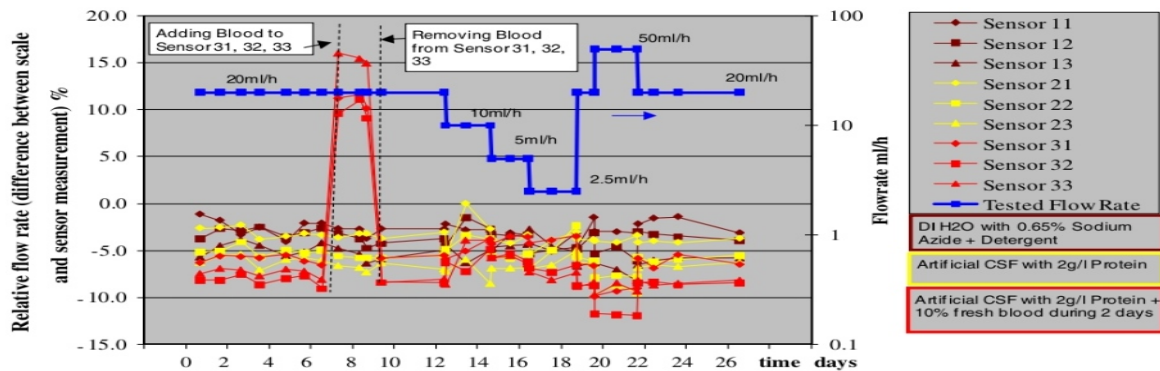


Figure 23: relative flow rate over 26 days with different scenarios

22°C calibrated sensor has offset of -5.4%. 37°C calibrated sensor has offset of + 6.3%. The compensation average for all relative flow rates is 0.9%. We notice that there is no major difference in the relative flow rate with changing the flow rate from 2.5 ml/h to 50 ml/h all readings are between ( 0% and 10% offset).

Different orientations for the sensor were made to ensure the reliability of the readings for the patient in different positions combined with tilt sensor data the patient position is confirmed and the opening pressure is adjusted.

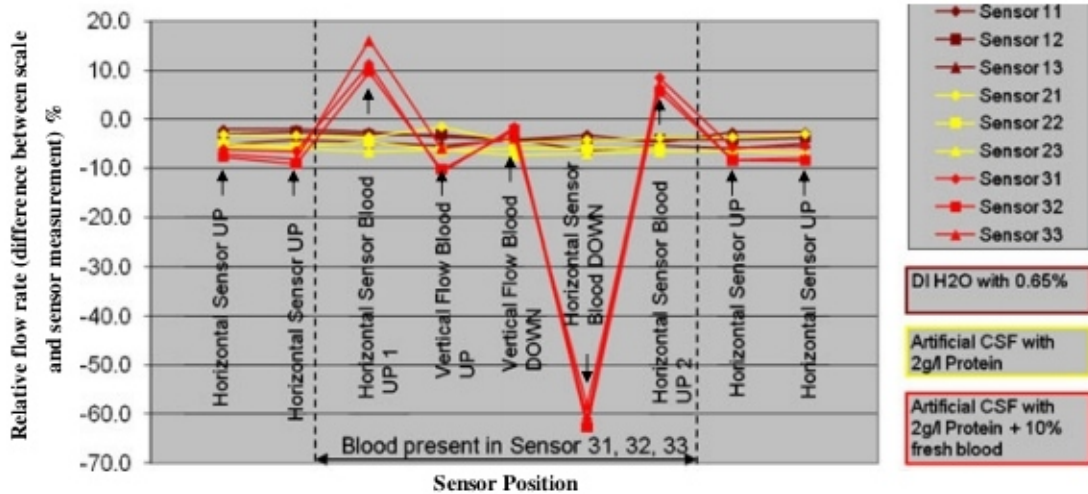


Figure 24: different positions for the sensor and flow direction

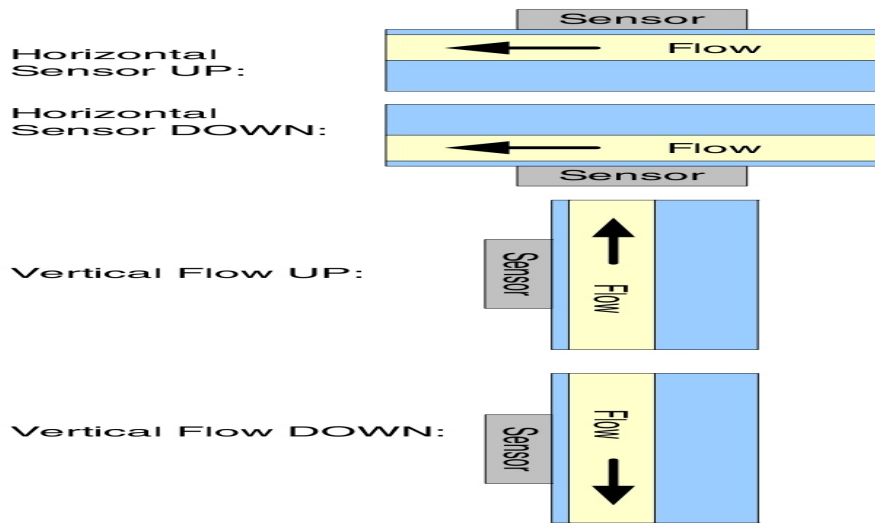


Figure 25: relative flow rate with different positions

These results show when no blood in the CSF, the orientation of the sensor does not affect the readings.

The sensor depend on thermal conductivity of the liquid in contact with. The results in 23 & 25 depend on stored calibration curve for water. Another liquid ( big different thermal conductivity ) will mess the results.

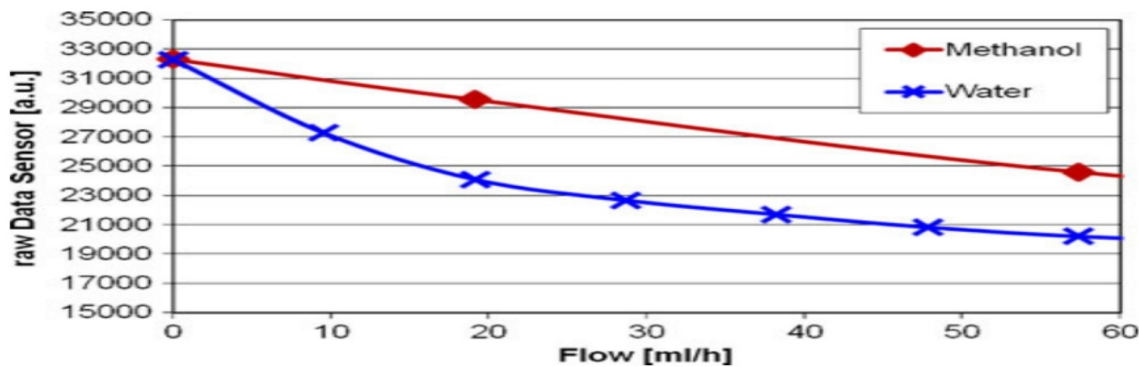


Figure 26: calibration curves for calorimetric flow sensor with different thermal conductivity fluids

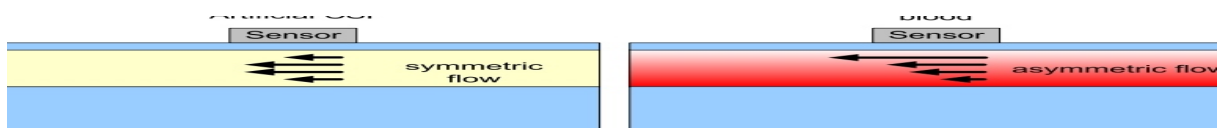


Figure 27: (left)artificial CSF symmetric flow (right) asymmetric flow in the presence of blood

## 6.5 Accuracy, Precision, And Uncertainty

### Accuracy

The accuracy ranges from -2 % to -10 % with an average -5.4%. It is calculated by relative flow rate equation over 26 days

$$\text{relative flow rate} = \frac{\text{flow rate(sensor)} - \text{flow rate(scale)}}{\text{flow rate(scale)}} \times 100\%$$

For sensor calibrated at 37°C accuracy is -5.4%. For sensor calibrated at 22°C accuracy is +6.3%. With and without blood added the accuracy ranges from -5% to -9%.

### Precision

there are different methods to calculate the precision we will use a manual method with low number of values and do it manually. Better precision calculation will be using a numerical method

$$\text{precision} = \text{mean} \pm \text{deviation}$$

$$\text{deviation} = \frac{\sum_{i=1}^n (x_i - \text{mean})}{n}$$

$$\text{precision} = -5.4\% \pm 2.9\%$$

### uncertainty

The uncertainty will be very hard to be calculated manually as it sum the error of all parameters the general equation is:

$$\text{uncertainty} = \sqrt{\left(\frac{\Delta x}{x}\right)^2 + \left(\frac{\Delta y}{y}\right)^2 + \left(\frac{\Delta z}{z}\right)^2 + \dots}$$

and x, y, z are different parameters for each equation implemented earlier.

## 7 Intercranial Pressure memo sensor

The Cerebrospinal Fluid (CSF) in brain has a minimal Intercranial pressure of 7–15 mmHg. There is an index been used to indicate any changes in the normal ICP range is called RAP; it represents a correlation between the amplitude and the mean value of the ICP. It is normal ICP, if the RAP index is close to zero and indicates a good compensatory reserve. A RAP that is > 0.6 indicates a poor compensatory reserve.

If we want to monitor the ICP in terms of mmHg, it has to be during sleep while the body is in horizontal plane. During a normal 8-hour sleep, if the average ICP is < 12 mmHg, then it's in normal range. While from 12 – 15 mmHg, we can say it's at the borderline. But once it's above 15 mmHg, it's interpreted as elevated pressure.

## 7.1 Device Design

### 7.1.1 Components

The Device is composed of 1) a pressure sensor interface, 2) power management circuits, 3) and other components in order to convert the pressure sensor output into signals that can be transmitted wirelessly.

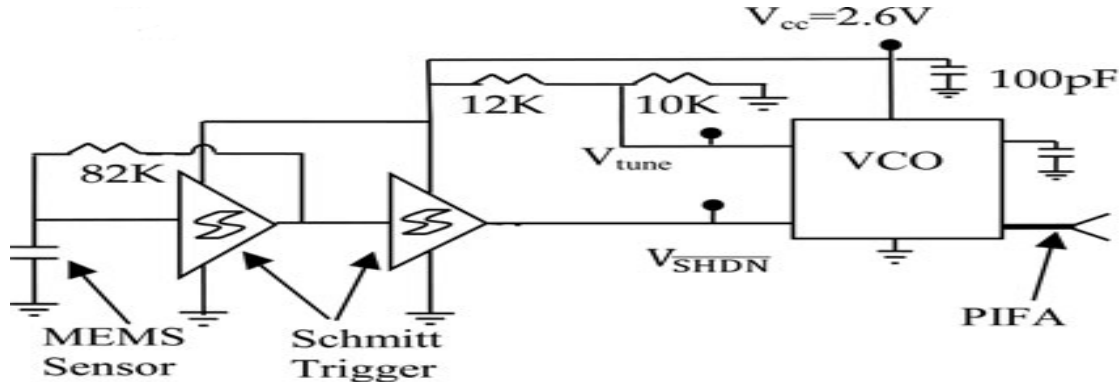


Figure 28: schematic circuit for the pressure sensing device.

fig(28)shows the schematic circuit for the pressure sensing device.

- The MEMS sensor is a capacitive pressure sensor that is responsible for capturing the pressure values.
- The Schmitt Triggers are comparator circuits that are implemented by using positive feedback non-inverting amplifiers and their job is to convert analog input into digital output signal and it is used to modulate a 2.4 GHz RF oscillator.
- VCO is a voltage-controlled oscillator.
- PIFA is a planar inverted F antenna which is coupled to the Schmitt Triggers.

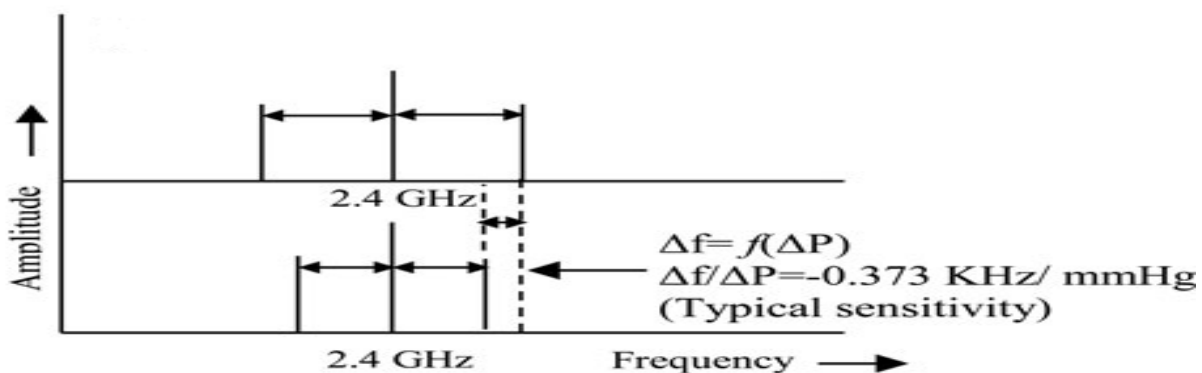


Figure 29: the frequency characteristics of the device

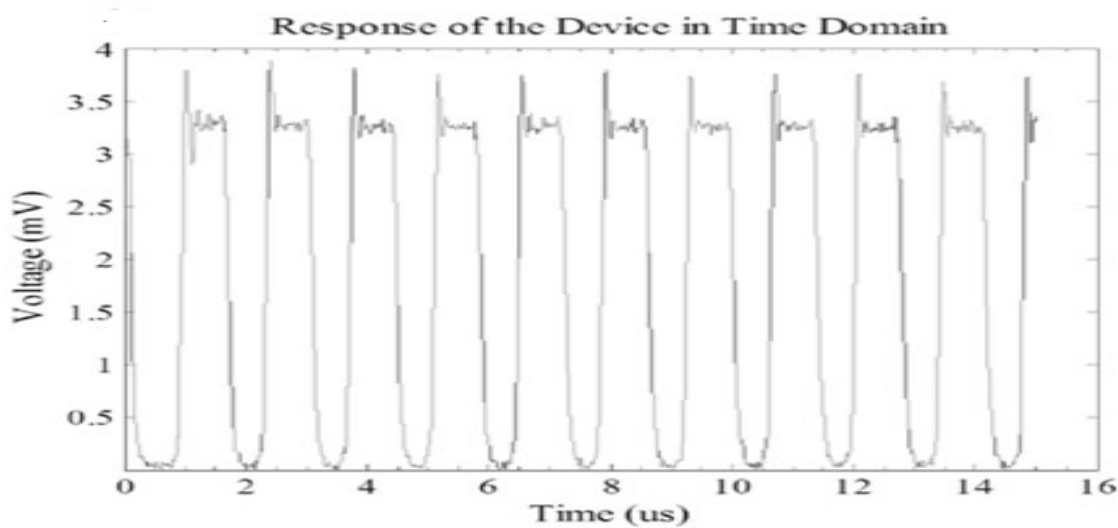


Figure 30: the response of the device in time domain.

### 7.1.2 Fabrication

The Device Components are assembled inside a cylindrical metal case with the dimensions: diameter of 12 mm, height of 10 mm, and a conduit of 4.5 mm at the base. And the pressure sensor is placed at the bottom open end of the conduit, so that the pressure sensing end is exposed at all time to the flow of CSF. All the components are kept inside a medical grade epoxy and sealed with biograde silicone. The final step in the fabrication process is that a coating of parylene (2.5  $\mu\text{m}$ ) is applied in order to maintain the biocompatibility and the integrity of the device.



Figure 31: fabricated device

### 7.1.3 calibration

The device is calibrated in an 8-day process in three different steps; the first one is in dry conditions at 25°C and the second one is in wet conditions at (30-37)°C, finally, in hydrostatic medium at (36-37)°C. It was found that the sensitivity of measurement was

less than 1 mmHg and the zero drift is less than 2 mmHg, with a max estimated error of 4.86% of the full scale

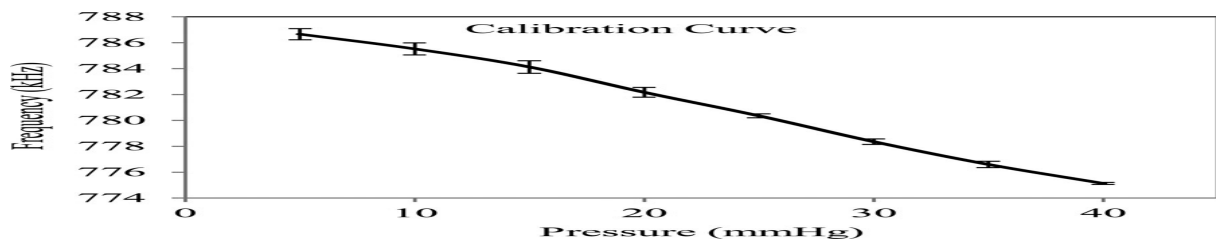


Figure 32: calibration curve

## 7.2 principle of working of pressure sensor

two conducting layers are deposited on a diaphragm to creat a capacitor. pressure added change the spacing between the two layers which change the capacitance. the change is measured by adding the sensor with a tuned circuit that change its frequency with pressure. additional electronics added turn it to an oscillator which is optimal for wireless data transmission with the help of antenna technology.

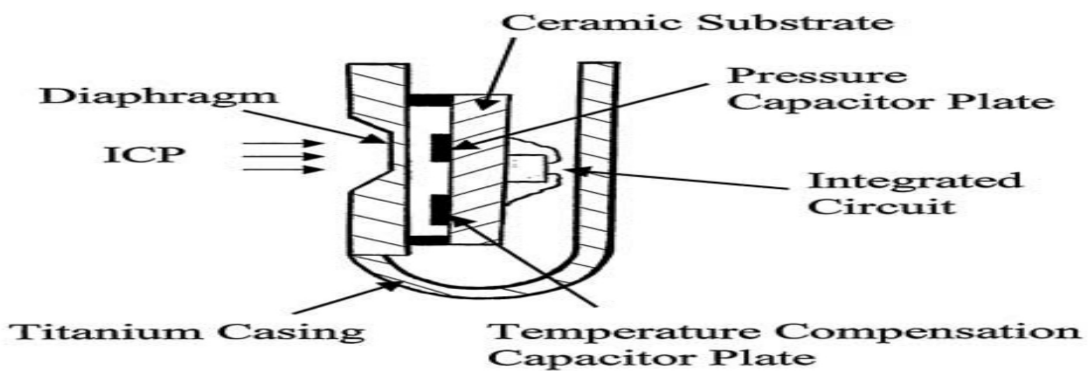


Figure 33: pressure sensor

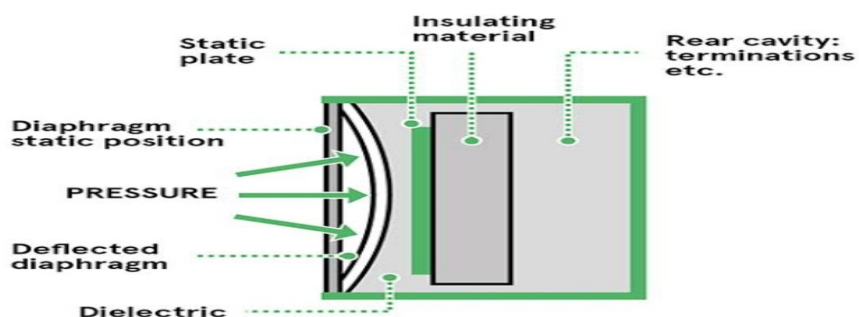


Figure 34: principle of working

## 8 micro capacitive tilt sensor

Tilt sensor is considered an important device in determining human directions, it helps in determining and following the patient's level of recovery ,Because of only the tilt sensor is somewhat complicated so some chemical and biological sensors can be combined with it, such as glucose or the PH, to measure physical and biochemical changes simultaneously, despite all attempts to improve the performance of the tilt sensor, but it is the range and performance in the angle deviation were not sufficiently accurate so that the MEMS was The best solution to overcome all these obstacles like a simple small design, low cost and lower consumption. Some accelerometer can be used as a tilt sensor, but still, the resolution is not high enough, and the range is limited.



Figure 35: body movement detection, MEMS tilt sensor at limb joints to monitor several motion parameters continuously



Figure 36: a necklace and monitors tiny movements to improve your posture

### 8.1 Initial Design

The tilt sensor consists of a fixed block, a comb drive capacitors and a moving rod in one direction only and cannot move in other directions as shown in fig37.

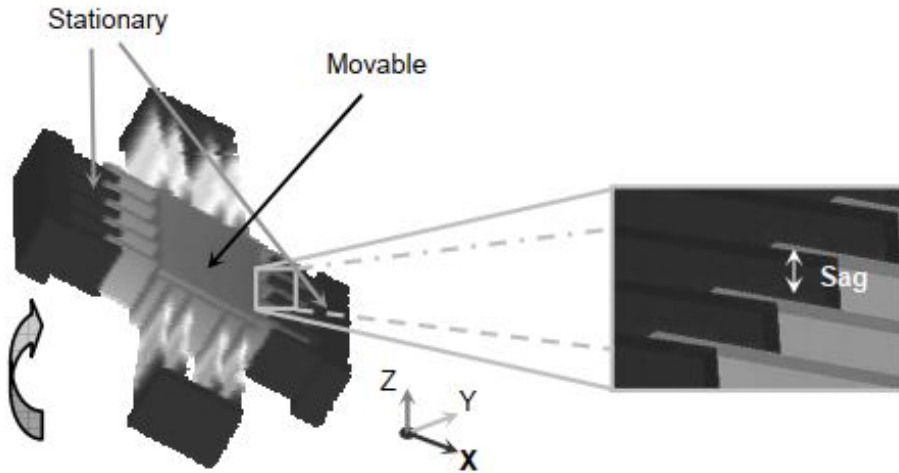


Figure 37: The interior design of the tilt sensor demonstrating the comb capacitors, the fixed beam and the movable beam

## 8.2 Principle of working

When rotation occurs in a certain direction, gravity forces the moving rod to go toward the first fixed bar while moving away from the other. This causes the change in capacitance to occur, and there are increasing on the side that the moving rod moves toward, and decreasing on the other side, then The differential capacitance  $|C_{right} - C_{left}|$ . An intensive comb capacitance idea is an effective idea to get a large capacity and miniaturization, the previous design can be also a displacement sensor which is related with the capacitance, so we will show the equation that links the relation between the angle of rotation and the capacitance.

$$C = \frac{(I_o \pm \Delta x)h\epsilon}{G}N = \frac{A_o\epsilon}{G}N$$

$$\Delta x = \frac{mg \sin \theta}{K_x}$$

, where:

- C is the capacitance.
- $I_o$  initial overlap length of the finger pairs.
- h is the thickness.
- G is the gap width.
- N is number of finger pairs.
- $\epsilon$  is permittivity of the medium.

- $A_o = (I_o \pm \Delta x)$  is the overlap area.
- $mg$  is the gravitational force.
- $K_x$  is the spring constant.
- $\Delta x$  is lateral displacement.

So to increase the capacitance we should increase the aspect ratio ( $AR = \frac{h}{G}$ ) and N (the number of the pair plates) we can do that without increase the size of sensor by increasing the number of combs, there are an important point that after a period of time the rigidity decreases so the displacement will increase subsequently the capacitance difference will increase .fig38 shows the variation of differential capacitance  $|C_{right} - C_{left}|$  and the tilt from  $0^\circ$  to  $90^\circ$ .

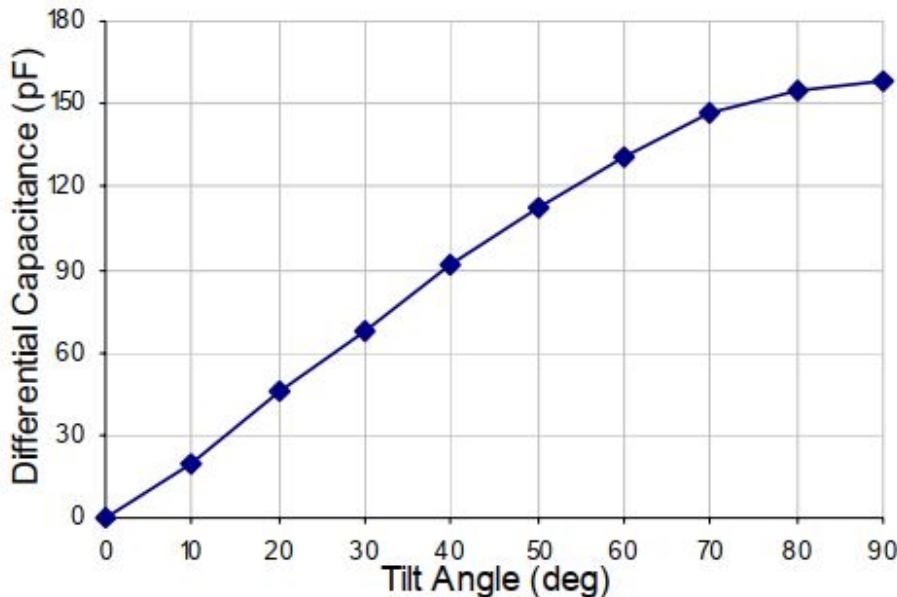


Figure 38: relation between capacitance  $|C_{right} - C_{left}|$  and tilt angle

As we see in fig38 the relation is not linear and this may be make some disadvantages like less resolution and increase the range of the tile reading .there are some method to improve the linearization the first one is re shape the beam but this method may decrease the capacitance, the second method is to increase the total sage or plates, by this method will increase the capacitance and this will treat the problem of the first method. If we combined the two method we will overcome the problem of linearization between the difference capacitance and the tilt angle.

### 8.3 Digital Sensor

MEMS is used in variable devices like accelerometer to determine the displacement ,and it can do that by changing the capacitance, the total capacitance will depend on the size of the device.

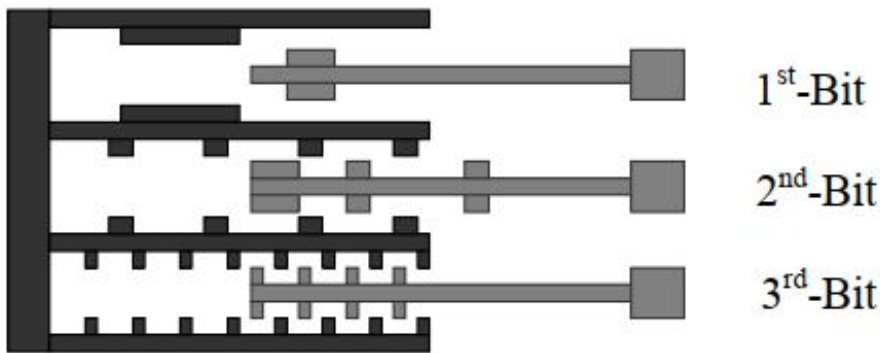


Figure 39: Schematic of a 3-bit digital comb

So we can design tilt sensor with digital comb capacitors , it is formed of a fixed plates like teeth and a movable plate also like teeth every stage different in the number of plates and the radius of the plate as shown in the previous figure , this will make the implementation of the output very easy by using a binary reader , also we can detect each bit by using a binary comparator either between differential capacitors or a using a threshold value, so we can read the three bits without processing by using binaryreader . as in the traditional one it Is important to make the variation in the capacitance big to have a big resolution to sense the small tilt ,there are a problem is called Fringing field effects or edge effect that decrease the difference capacitance, as we show the flux between the two plate is regular and liner at this point there is no problem the problem is these nonlinear flux that get out from the tow plates for first second you may thought that this unregulated flux increase the capacitance but the opposite is the true ,as we know the total charge  $q$  is constant so fringe field make another capacitor between the wire that conducting and between the capacitor in between.

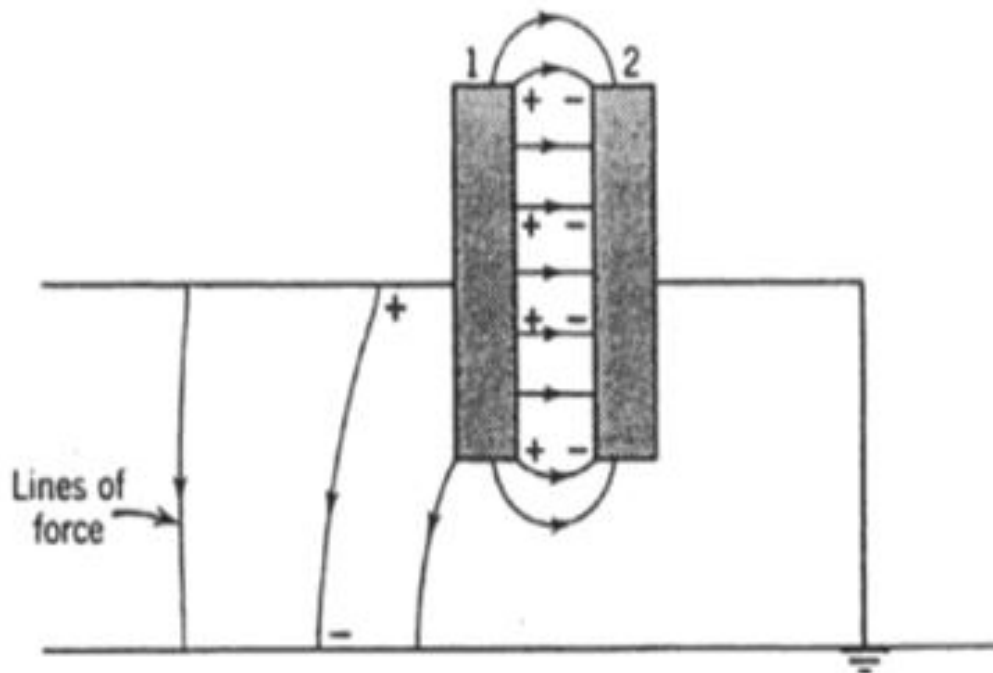


Figure 40: Fringing field or edge effect effects between two plates

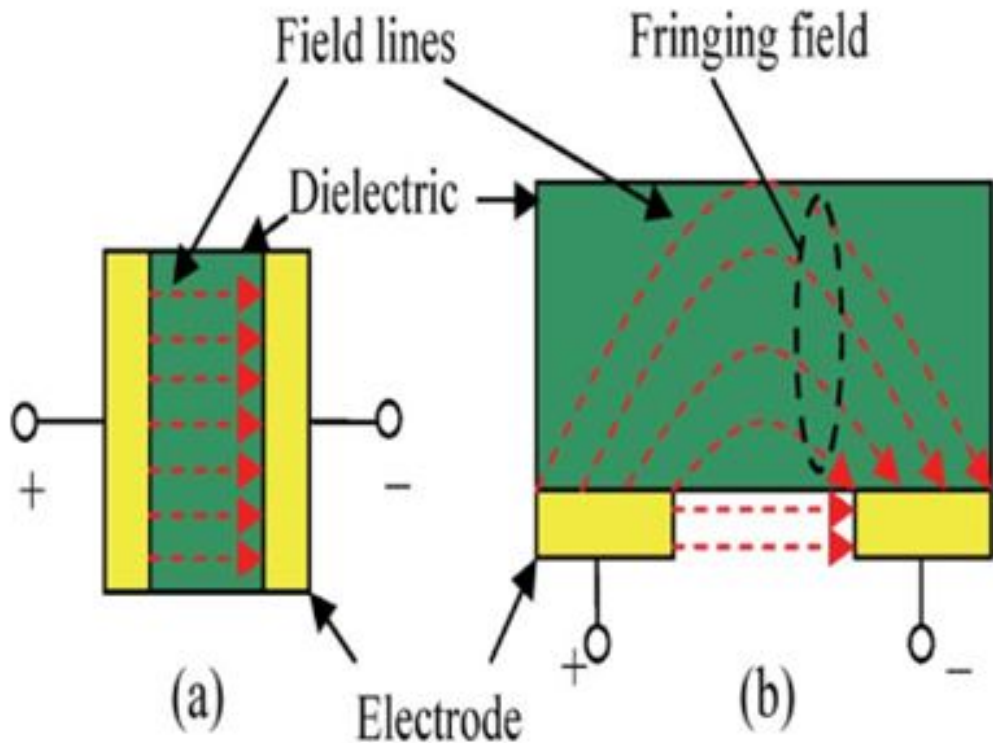


Figure 41: Fringing field or edge effect affects the adjacent plate

So there is a method to avoid that is to increase the distance between teeth, as we see

in the fig42 the more we increase the teeth gap the more capacitance difference increase.

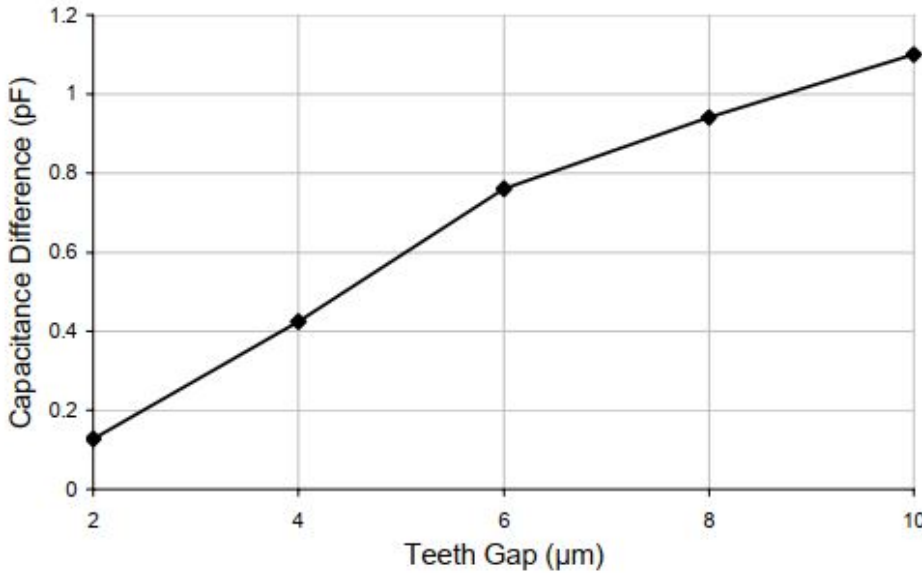


Figure 42: show the relation between the capacitance difference and the teeth gap

But by increasing the gap width the comb length will increase so as a compromise between device size and sensitivity the gap width will be  $6 \mu M$ .

## 8.4 Resolution, Precision, And Accuracy

### Resolution

From the previous graph in the fig38 we can calculate the resolution

Note: we will do that after making the linearization

$$\text{Resolution} = \frac{(90 - 20)}{(40 - 10)} = 2.333 \text{PF/}^\circ$$

### Precision

There are various methods to calculate the Precision we will take the numerical one by calculating the average deviation after taking a number of reading suppose reading is (11, 13, 12, 14, 12). The mean will be equal to 12.4 degree and then calculate the absolute deviation ( $x - m$ ) then calculate the average deviation .

average deviation =  $\frac{\sum |x - \mu|}{n}$  standard deviation = 1.3, so the precision result =  $12.4^\circ \pm 1.3^\circ$ .

### Accuracy

from

$$\% \text{error} = \frac{(\text{measured value} - \text{true value})}{\text{true value}} * 100$$

we can calculate the accuracy from the previous equation by making the calibration several times at different position and condition, we found that the accuracy is equal to  $\pm 0.1^\circ$

from the full scale

## 9 Wireless body communication

Wireless body area network(WBANS) is a technology that help us to monitor the condition of the patient everywhere at any time it is a group of medical devices or motion detectors that are on ,in or around the body advanced health care devices are used in the body to reduce the invasiveness of the medical procedure number.

There are sensor that shown in 43 used to monitor the data to the hospital information system (HIS).

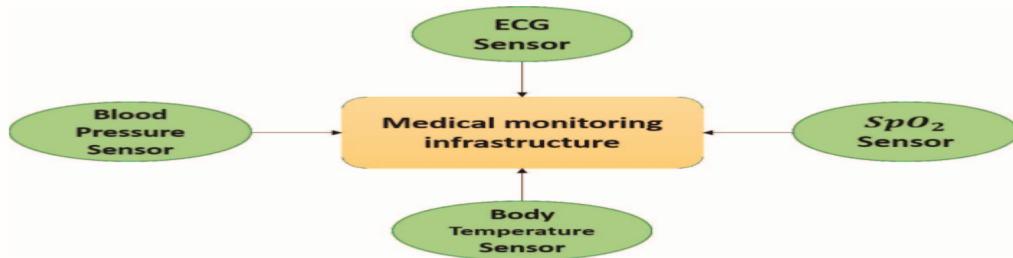


Figure 43: Sensor network of biomedical monitoring applications

We can use these sensors later to monitor the chemical substances percentages as hemoglobin and the insulin this will be very useful for long term disease.

The in vivo networking for WBANS is considered as an important application that help in continuous wireless enabled healthcare and also known as the intra body communication (IBCS) internal health monitoring and internal drug administration are examples of application that need to in vivo sensors to transmit to the body surface receiver.

### 9.1 Art of in vivo communication

In vivo communication is a type of signal transmission that uses the human body as transmission medium for electrical signals the induction of the electrical current is enabled into the human tissue through the modern transmission devices 44 shows the main component of an in vivo communication link.

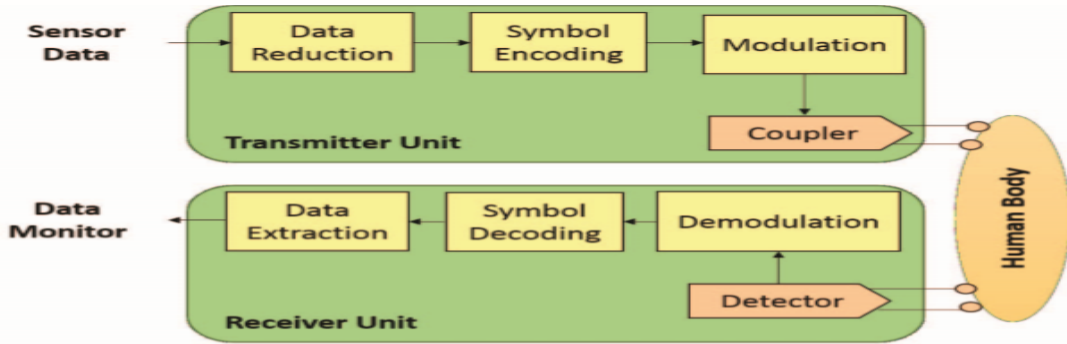


Figure 44: In vivo communication for data transmission between sensors enabled by transmitter and receiver units

The transmission unit used to compress and encode the data then transfer it by the current controlled coupler unit the human body acts a transmission unit electrical signals can pass through the tissues.

On the other had the reviewer unit composed of analog detector unit that amplifies the received signal for demodulation and extraction.

From here we that it is possible to transmit the electrical signal through the body but we should be Cautious about the tissues from the effect of the electrical signal .

## 9.2 In vivo channel modeling and characterization

There are differences in the signal velocity between the body organs and this attenuate the signal and make losses in the quality of the signal<sup>45</sup>.

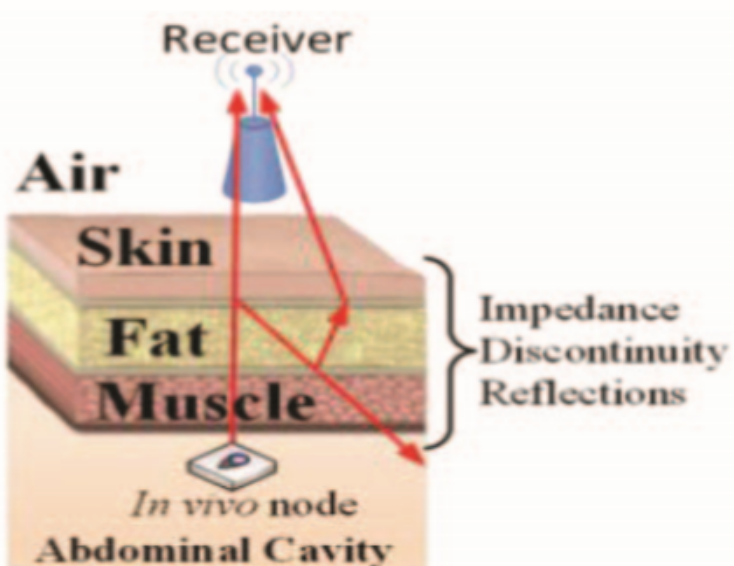


Figure 45: In vivo multi-path channel

In addition due to the antenna are radiated to the losing medium in addition to the loss of environment nearer electrical fields differs from the far one for this reason the signal need to different equations to calculate its characteristics

Many experiments are done to determine the difference between the receiver position in the body or on the surface modeling the in vivo wireless channel and phenomenological path loss model is one of the new research goals in this field.

A-path loss: There are two methods to calculate the path loss the first one is to use the Hertzian-Dipole antenna the second one is to use the mono pole antenna. The Hertzian-Dipole antenna we can calculate as follows

$$\text{path Loss}(r, \theta, \phi) = 10 \log \frac{|E|_{r=0}^2}{|E|_{r,\theta,\phi}^2}$$

where:

- r is distance from origin.
- $\theta$  is polar angle.
- $\phi$  is azimuth angle.
- E is field of origin.

The mono pole are good choice because they are small and multi directional the path loss can be measured by the scattering parameters( S parameter ).

$$|S_{21}|^2 = \frac{P_r}{P_t}$$

$$\text{Pathloss}(dB) = -20 \log |S_{21}|$$

. where:

- $P_r$  is the received power.
- $P_t$  is the transmitted power.

the defines the relation between the input and the output in the electrical system if we make port 1 transmit antenna and port 2 the receive antenna then S21 is the power gain this according to 46

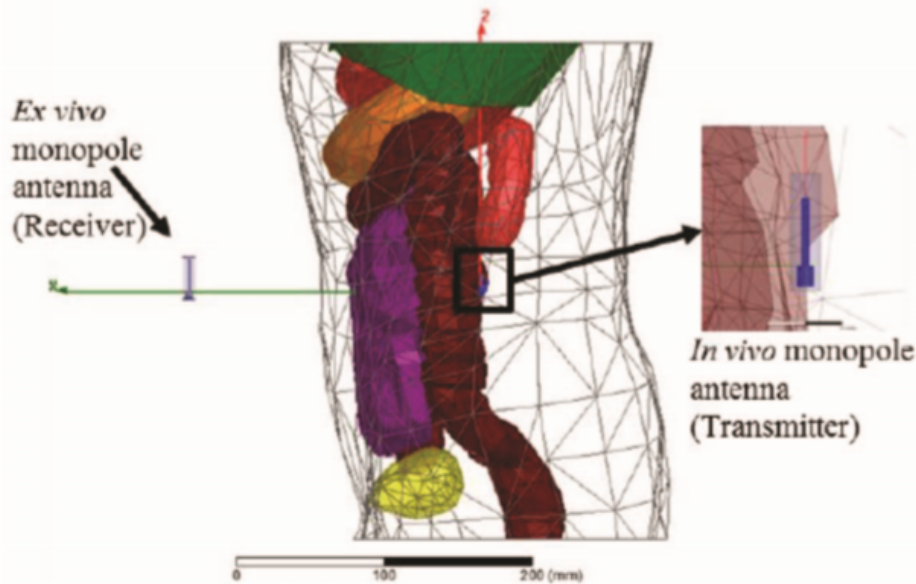


**Fig. 6.** Simulation setup by using monopoles to measure the path loss

Figure 46: Simulation setup by using monopoles to measure the path loss

Finally, we can monitor this data in our demo project by arduino using Bluetooth module.

### 9.3 Wireless powering of medical sensors

We will discuss the wireless electricity (wiricity) which can help us in providing power to medical sensors .there are many battery powered implantable medical devices as infusion pumps and cardiac assist pumps and pacemakers . . . etc.

Transcutaneous magnetic induction system have some drawbacks as short operating distance and low power transfer efficiency so the problem of power supply in implanted medical sensors (IMDS) remains a technical change.

This problem affects not only the (IMDS) but also affects on the non-invasive sensors because the battery add weight and size to the sensor and this take a much effort in maintenance.

Recently wiricity used to illuminate a 60w light bulb from 7 feet away the power efficiency achieved was 40%using two identical resonant coils of 60cm in diameter this experiment used in consumer electronics as computers, laptops and phones but is still unused in medical application.

**Theory of wiricity system:** Wiricity is based on the near field strongly coupled magnetic resonance the main principle is that the resonant object exchange energy efficiently and the non-resonant interact weakly .wiricity system is composed of two resonators driving

loop and output loop the source is attached to the output loop linked to the oscillators to obtain the energy .similarly the device coil with supply to an external load as shown in figure(??)Basic components of witricity system.)



Figure 47: Basic components of witricity system

### 9.3.1 The effect of the environment

As we know that the environment may less the interacting between the source and the device so we can fill the near field with lossless non radiative magnetic fields oscillating at MHZ and this will make the interaction between the source and device efficient from here we can build a wireless channel for power transmission.

Practically , we use a thin belt shaped resonator by putting it on the out cover or inside the cover of the medical device and this can provide a space for the device and facilitates heat dispersion.

### 9.3.2 Experimental results

First experiment we used a led and connected to the output loop and we then tuned the frequency at 6.9 MHZ when we put the receiver directly above the transmitter the led was light. Figure(48).And we put the receiver in a plastic head we noticed that the led was also light as we saw in the last experiment.

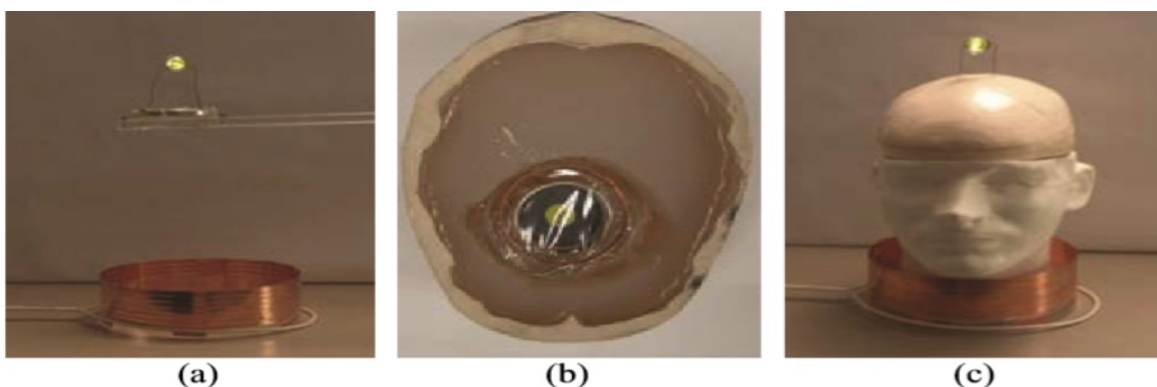


Figure 48: . In vitro experimental results (a) through open air (b) with receiver implanted in agar "brain" (c) through the head model

## 10 discussion

the flow rate sensor calibrated at different temperature ( $22^{\circ}\text{C}$  , $37^{\circ}\text{C}$ ) has different affects range from (0% to 10%) no matter the slow rate is  $2.5\text{ml/hor}$  up to  $50\text{ml/h}$ . the orientation also doesn't affect the readings. the tilt sensor provide a lot of information about the patient like walking ,sleeping ,sitting or suddenly fall. the pressure sensor is important for monitoring the ICP . if it increases over 12 mm/Hg that mean that the patient in danger . the device was calibrated in different media with sensitivity less than 1 mm/Hg

## 11 conclusion

Implantable flow sensor is a revolutionary way for improving the quality of the shunt and better care for the patient with optimal regulation of the flow.

Calibrating the sensor at different temperatures or fluids will cause drift by an average -5.4% for the calibrated device at  $22^{\circ}\text{C}$  and 6.3% for the calibrated device at  $37^{\circ}\text{C}$ . Different positions does not affect the readings.

Pulse width should have a duty cycle 15% to 20% to reduce the power dissipation. Proper software in the external unit reduce the power dissipation in the implant. MEMS tilts sensor is based on digital com capacitors , despite the digital sensor is composed of 3 bit there are some application can be done for example patient monitoring system , when the other sensor like pacemaker or flow sensor of pressure sensor are working the tilt MEMS is also working and gives a lot of information about patient like walking ,sleeping, suddenly fall .the resolution is very important but less than power consumption ,where the whole package sensor is derived by small power supply, it can also used in the imaging like x-ray or CT as the patient should take specific posture during imaging ,beside that we can use it in the robot design.

CSF absorption depend on difference between ICP and dural sinus pressure. Head lower than the heart also affect absorption. If the head is down by  $20^{\circ}$  for 10 min , LVP and SSP increase but return back to normal quickly in the horizontal position. ICP increase 3 times more than normal if the head is inverted see fig49

**Table 1.** Effect of Head-Down Tilt on Cerebrospinal Fluid and Blood Pressures.<sup>a</sup>

Horizontal Position (Control)	Head-Down Tilt (min)							Return to Horizontal Position
	10	20	40	60	80	100	120	
LVP	4 ± 0	12 ± 1 <sup>b</sup>	11 ± 1 <sup>b</sup>	4 ± 1				
SSP	-2 ± 0	5 ± 0 <sup>b</sup>	-2 ± 0					
ECSFP	7 ± 1	9 ± 0	8 ± 1	8 ± 1	8 ± 1	8 ± 1	9 ± 1	7 ± 1
MAP	83 ± 3	93 ± 2 <sup>b</sup>	93 ± 4 <sup>b</sup>	93 ± 4 <sup>b</sup>	94 ± 5 <sup>b</sup>	90 ± 8	89 ± 8	84 ± 5

LVP, lateral ventricular pressure; SSP, sagittal sinus pressure; ECSFP, effective cerebral spinal fluid pressure; MAP, mean arterial pressure.

<sup>a</sup> End value is the mean pressure in mm Hg ± standard error.

<sup>b</sup> P < 0.01 versus control.

Figure 49: effect on ICP, LVP, SSP, ECSFP, and MAP with head tilt

The passive effects of ICP elevation does not show immediately so it is important to alert the patient if he stayed in wrong position for along time.

ICP increase over 15 mmHg may lead to brain injury, seizure, coma, stroke or death. Some symptoms may appear on the patient like headache, pupil response decrease, sleepiness, vomiting, and confusion. ICP increase in infants may cause skull sutures to separate and soft plates to move apart.

For the CSF production and flow rate 125 ml of CSF is presented at any given time. 500 ml/day are produced(25 ml/h). This fluid is constantly absorbed so only 125 ml is presented. Our device is used to alert the doctor and the patient if any of the values exceeded the normal ranges allowing the doctor to adjust or provide some instructions to the patient without rushing to the hospital. Overdrainage may cause ventricle to shrink, cause it to be displaced or cause atrial rupture.

## References

- [1] T. Bork, Thermal Flow Sensor Having Streamlined Packaging, US Patent No. 7,181,963 B2 (2007)
- [2] H.L. Brydon, G. Keir, E.J. Thompson, R. Bayston, R. Hayward, W.Harkness, J. Neurol. Neurosurg. Psychiatry 64, 643 (1998)

- [3] M. Critchley, J.L. O'Leary, B. Jennett, *Scientific Foundations of Neurology*, 1st edn. (Heinemann Medical, London, 1972)
- [4] H. Davson, M.B. Segal, *Physiology of the CSF and Blood-brain Barriers*, 1st edn. (CRC, New York, 1996)
- [5] A. Ginggen, Method for brazing two glass components, European Patent No. EP1184351 (2003)
- [6] A. Ginggen, Y. Tardy, R. Crivelli, T. Bork, P. Renaud, Biomedical Engineering, *IEEE Trans. Biomed. Eng.* 55(4), 1374 (2008)
- [7] International Standards Organization (ISO) 14708-1. Implants for surgery—Active implantable medical devices—Part 1: general requirements for safety, marking and for information to be provided by the manufacturer (2000)
- [8] F. Mayer, A. Häberli, H. Jacobs, G. Ofner, O. Paul, H. Baltes, Proc.IEEE International Electron Device Meeting IEDM 97, IEEE 1997, p. 895-898. (1997)
- [9] Chen, Z. Fan, J. Zou, J. Engel, and C. Liu, "Two-dimensional micromachined flow sensor array for fluid mechanics studies." *Journal of Aerospace Engineering*, vol. 16, pp. 85-97, 2003
- [10] Fraden, "Flow Sensors," in *Handbook of Modern Sensors*, 4th edition. New York, NY: Springer New York, 2010, chapter 11, pp. 399-429.
- [11] T. Ebefors, E. Kalvesten, and G. Stemme, "Three dimensional silicon triple-hot-wire anemometer based on polyimide joints," *Proceedings MEMS 98. IEEE. Eleventh Annual International Workshop on Micro Electro Mechanical Systems. An Investigation of Micro Structures, Sensors, Actuators, Machines and Systems (Cat. No.98CH36176)*, pp. 93-98, 1998.
- [12] Bloom HJ: Surgical repair of the cleft palate. In: Archer WH, ed: *Oral and Maxillofacial Surgery*, Vol II. Philadelphia, WB Saunders Co., 1975;1849-1859.
- [13] 1. Bloom HJ: Surgical repair of the cleft palate. In: Archer WH, ed: *Oral and Maxillofacial Surgery*, Vol II. Philadelphia, WB Saunders Co., 1975;1849-1859.
- [14] Rheault W, Derleth M, Casey M, Czarnik C, Kania D, Nagel G: Effects of an inverted position on blood pressure, pulse rate, and deep tendon reflexes of healthy young adults. *Phys Ther* 1985;65:1358-1362.
- [15] H.Kawamoto, "A Study of Capacitance Type Incline Sensor," *Institute of Electric and Electronics Engineering of Japan*, vol. R83-56, pp. 13-18, 1984

- [16] Zhao, L., & Yeatman, E. M. (2007). Micro capacitive tilt sensor for human body movement detection. In 4th International Workshop on Wearable and Implantable Body Sensor Networks (BSN 2007) (pp. 195–200). Springer, Berlin, Heidelberg.
- [17] A. Marmarou, “Increased intracranial pressure in head injury and influence of blood volume,” *J. Neurotrauma*, vol. 9, pp. S327–S332, Mar. 1992.
- [18] M. Kiefer, S. Antes, S. Leonhardt, M. Schmitt, B. Orakcioglu, O. W. Sakowitz, and R. Eymann, “Telemetric ICP measurement with the first CE-approved device: Data from animal experiments and initial clinical experiences,” *Acta. Neurochir. Suppl.*, vol. 114, pp. 111–116, 2012.
- [19] G. Silasi, C. L. MacLellan, and F. Colbourne, “Use of telemetry blood pressure transmitters to measure intracranial pressure (ICP) in freely moving rats,” *Curr. Neurovasc. Res.*, vol. 6, pp. 62–69, Feb. 2009.
- [20] L. Salvador, R. Valero, J. Carazo, L. Caral, J. Rios, E. Carrero, J. Tercero, N. de Riva, P. Hurtado, E. Ferrer, and N. Fabregas, Pressure inside the neuroendoscope: Correlation with epidural intracranial pressure during neuroendoscopic procedures, *J. Neurosurg. Anesthesiol.*, vol. 22, pp. 240–246, Jul. 2010.
- [21] M. A. Poca, J. Sahuquillo, T. Topczewski, M. J. Penarrubia, and A. Muns, “Is intracranial pressure monitoring in the epidural space reliable? Fact and fiction,” *J. Neurosurg.*, vol. 106, pp. 548–556, Apr. 2007.
- [22] P. K. Eide, “Comparison of simultaneous continuous intracranial pressure (ICP) signals from ICP sensors placed within the brain parenchyma and the epidural space,” *Med. Eng. Phys.*, vol. 30, pp. 34–40, Jan. 2008.
- [23] J. Zhong, M. Dujovny, H. K. Park, E. Perez, A. R. Perlin, and F. G. Diaz, “Advances in ICP monitoring techniques,” *Neurol. Res.*, vol. 25, pp. 339– 350, Jun. 2003.
- [24] B. A. Gregson, K. Banister, and I. R. Chambers, “Statistics and analysis of the Camino ICP monitor,” *J. Neurol. Neurosurg. Psychiatry*, vol. 70, p. 138, Jan. 2001.
- [25] S. Shapiro, R. Bowman, J. Callahan, and C. Wolfla, The fiberoptic intraparenchymal cerebral pressure monitor in 244 patients, *Surg. Neurol.*, vol. 45, pp. 278–282, Mar. 1996.
- [26] M. Chavko, W. A. Koller, W. K. Prusaczyk, and R. M. McCarron, “Measurement of blast wave by a miniature fiber optic pressure transducer inthe rat brain,” *J. Neurosci. Methods*, vol. 159, pp. 277–281, Jan. 30, 2007.

- [27] R. A. Weerakkody, M. Czosnyka, C. Zweifel, G. Castellani, P. Smielewski, K. Brady, J. D. Pickard, and Z. Czosnyka, "Near infrared spectroscopy as possible non-invasive monitor of slow vasogenic ICP waves," *Acta. Neurochir. Suppl.*, vol. 114, pp. 181–185, 2012.
- [28] J. Bellner, B. Romner, P. Reinstrup, K. A. Kristiansson, E. Ryding, and L. Brandt, "Transcranial doppler sonography pulsatility index (PI) reflects intracranial pressure (ICP)," *Surg. Neurol.*, vol. 62, pp. 45–51, Jul. 2004.
- [29] P. Honeine, F. Mourad, M. Kallas, H. Snoussi, H. Amoud, and C. Francis, "Wireless sensor networks in biomedical: Body area networks," in *Systems, Signal Processing and their Applications (WOSSPA)*, 2011 7th International Workshop on, May 2011, pp. 388–391.
- [30] D. Cypher, N. Chevrollier, N. Montavont, and N. Golmie, "Prevailing over wires in healthcare environments: benefits and challenges," *Communications Magazine, IEEE*, vol. 44, no. 4, pp. 56–63, April 2006.
- [31] T. Ketterl, G. Arrobo, A. Sahin, T. Tillman, H. Arslan, and R. Gitlin, "In vivo wireless communication channels," in *Wireless and Microwave Technology Conference (WAMICON)*, 2012 IEEE 13th Annual, April 2012, pp. 1–3.
- [32] M. S. Wegmuller et al., "Intra-body communication for biomedical sensor networks," Ph.D. dissertation, Diss., Eidgenössische Technische Hochschule ETH Zurich, Nr. 17323, 2007.
- [33] C. He, Y. Liu, T. Ketterl, G. Arrobo, and R. Gitlin, "Performance Evaluation for MIMO In Vivo WBAN Systems," in *RF and Wireless Technologies for Biomedical and Healthcare Applications (IMWS-Bio)*, 2014 IEEE MTT-S International Microwave Workshop Series on, Dec 2014, pp. 1–3.
- [34] A. Ruaro, J. Thaysen, and K. Jakobsen, Head-Centric Body-Channel Propagation Paths Characterization. *IEEE*, 2015.
- [35] E. Piel, A. Gonzalez-Sanchez, H.-G. Gross, and A. van Gemund, "Spectrum-based health monitoring for self-adaptive systems," in *SelfAdaptive and Self-Organizing Systems (SASO)*, 2011 Fifth IEEE International Conference on, Oct 2011, pp. 99–108.
- [36] E. Chow, B. Beier, Y. Ouyang, W. Chappell, and P. Irazoqui, High frequency transcutaneous transmission using stents configured as a dipole radiator for cardiovascular implantable devices, in *Microwave Symposium Digest, 2009. MTT '09. IEEE MTT-S International*, June 2009, pp.